

---

Electrical Engineering Theses

Electrical Engineering

---

Spring 4-30-2012

## Modeling Polarization and Capacitance Hysteresis of Ferroelectric Capacitors

Bikash Shrestha

Follow this and additional works at: [https://scholarworks.uttyler.edu/ee\\_grad](https://scholarworks.uttyler.edu/ee_grad)



Part of the [Electrical and Computer Engineering Commons](#)

---

### Recommended Citation

Shrestha, Bikash, "Modeling Polarization and Capacitance Hysteresis of Ferroelectric Capacitors" (2012).  
*Electrical Engineering Theses*. Paper 10.

<http://hdl.handle.net/10950/68>

This Thesis is brought to you for free and open access by the Electrical Engineering at Scholar Works at UT Tyler. It has been accepted for inclusion in Electrical Engineering Theses by an authorized administrator of Scholar Works at UT Tyler. For more information, please contact [tgullings@uttyler.edu](mailto:tgullings@uttyler.edu).

**MODELING POLARIZATION AND CAPACITANCE HYSTERESIS  
OF FERROELECTRIC CAPACITORS**

by

BIKASH SHRESTHA

A thesis submitted in partial fulfillment  
of the requirements for the degree of  
Master of Science in Electrical Engineering  
Department of Electrical Engineering

Dr. Ron J. Pieper, Ph.D., Committee Chair

College of Engineering and Computer Science

The University of Texas at Tyler  
May 2012

The University of Texas at Tyler  
Tyler, Texas.

This is to certify that the Master's Thesis of

BIKASH SHRESTHA

has been approved for the thesis requirement on  
March 9<sup>th</sup>, 2012  
for the Master of Science in Electrical Engineering

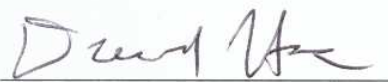
Approvals:



Committee Chair: Ron J. Pieper, Ph.D.



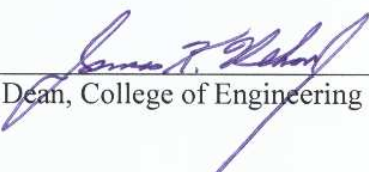
Member: Wudyalew Wondmagegn, Ph.D.



Member: David Hoe, Ph.D.



Chair: Department of Electrical Engineering



Dean, College of Engineering and Computer Science

## Table of Contents

List of Tables.....	iv
List of Figures.....	v
Abstract.....	vii
 1. Chapter 1: Introduction	
1.1 Ferroelectricity: Introduction, History and Applications.....	1
1.2 Literature Review.....	3
1.3 Objective.....	4
1.4 Thesis Organization.....	6
 2. Chapter 2: Background Study	
2.1 Perovskite Oxide and Ferroelectric Theory.....	7
2.2 P(VDF-TrFE).....	10
2.3 Experimental Ferroelectric Capacitor.....	11
2.4 Polarization Hysteresis Modeling.....	14
2.4.1 S. L. Miller <i>et al.</i> Model.....	14
2.4.2 Landau Free Energy Model for Monocrystalline Ferroelectrics...	17
2.4.3 J. Yu <i>et al.</i> Model.....	19
2.4.4 Y. L. Wang <i>et al.</i> Model for Polycrystalline Ferroelectrics.....	22
2.4.5 Modified Y. L. Wang <i>et al.</i> Model.....	26
 3. Chapter 3: New Models for Predicting Polarization	
3.1 Introduction .....	28

3.2 Model Based on Predicting Coefficients $\beta_1$ and $\beta_2$ .....	29
3.3 New Practical Model with Three-point Fit.....	31
3.4 New Practical Model with Four-point Fit.....	34
 4. Chapter 4: Capacitance Modeling	
4.1 Introduction.....	38
4.2 Large-Signal Capacitance Modeling.....	39
4.2.1 Using S. L. Miller <i>et al.</i> Model.....	40
4.2.2 Using New Four-point Fit Model.....	42
4.3 Small-Signal Capacitance Modeling.....	45
 5. Chapter 5: Conclusion and Future Work	
5.1 Conclusion.....	49
5.2 Future Work .....	50
5.3 Sponsor Acknowledgement.....	51
 References.....	52
Appendices.....	57
Appendix A: Mathematical Derivation for Finding $\delta$ in S.L. Miller <i>et al.</i> Model.....	57
Appendix B: Mathematical Derivation to Find $\alpha$ and $\beta$ for Landau Free Energy Model for Monocrystalline Ferroelectrics.....	59
Appendix C: Mathematical Derivation to Find $\delta^+$ and $\delta^-$ for J. Yu <i>et al.</i> Model..	61
Appendix D: Mathematical Expression for Generating Negative Going Branch Polarization Curve Using Four-point Fit Model.....	63
Appendix E: Mathematical Derivation for Small-Signal Capacitance.....	66

Appendix F: MATLAB Code for Polarization Hysteresis Using S. L. Miller <i>et al.</i> Model.....	68
Appendix G: Silvaco Code for Polarization and Capacitance Hysteresis Using S. L. Miller <i>et al.</i> Model.....	70
Appendix H: MATLAB Code for Polarization Hysteresis Using Landau Free Energy Model for Monocrystalline Ferroelectrics.....	72
Appendix I: MATLAB Code for Polarization Hysteresis Using J. Yu <i>et al.</i> Model.....	77
Appendix J: MATLAB Code for Polarization Hysteresis Using Y. L. Wang <i>et al.</i> Model.....	79
Appendix K: MATLAB Code for Polarization and Capacitance Hysteresis Using Model Based on Predicting Coefficients $\beta_1$ and $\beta_2$ .....	82
Appendix L: MATLAB Code for Polarization Hysteresis Using New Practical Model with Three-point Fit.....	84
Appendix M: MATLAB Code for Polarization and Capacitance Hysteresis Using New Practical Model with Four-point Fit.....	87
Appendix N: MATLAB Code for Large-Signal Capacitance Hysteresis Using Point to Point Numerical Derivative.....	92
Appendix O: MATLAB Code for Capacitance Hysteresis Using S. L. Miller <i>et al.</i> Model.....	94
Appendix P: MATLAB Code for Small-Signal Capacitance Hysteresis.....	95

## List of Tables

Table 2.1	Extracted values of the parameters from experimental polarization hysteresis.....	13
Table 2.2	Experimental values and corresponding Silvaco and MATLAB simulation parameters for model by S. L. Miller <i>et al.</i> .....	16
Table 2.3	Experimental and MATLAB simulation parameters for the model using Landau free energy theory for monocrystalline ferroelectric.....	19
Table 2.4	Experimental and MATLAB parameters for J. Yu <i>et al.</i> Model.....	21
Table 2.5	Simulation parameters for the polarization hysteresis of ferroelectric using Landau free energy expression by Y. L. Wang <i>et al.</i> .....	25
Table 2.6	Simulation parameters for the polarization hysteresis of ferroelectric using modified Y. L. Wang <i>et al.</i> model.....	27
Table 3.1	Values of the terms for calculating $\beta_1$ and $\beta_2$ .....	30
Table 3.2	Values of the terms for calculating $\beta_1$ , $\beta_2$ and $\beta_3$ .....	32
Table 3.3	Values of the terms for calculating $\beta_1$ , $\beta_2$ , $\beta_3$ and $\beta_4$ .....	35
Table 3.4	Values of the simulation parameters for polarization hysteresis of ferroelectric by using new practical model with four-point fit.....	36
Table 4.1	Values of MATLAB simulation parameters for small-signal capacitance modeling.....	48
Table D.1	Values of the terms for calculating $\beta_1$ , $\beta_2$ , $\beta_3$ and $\beta_4$ for negative going polarization curve.....	64

## List of Figures

Figure 2.1	Two different views of a unit cell of a perovskite oxide.....	7
Figure 2.2	Generation of polarization in a BaTiO <sub>3</sub> unit cell.....	8
Figure 2.3	Domains and domain walls (a) before poling and (b) after poling.....	9
Figure 2.4	Spontaneous polarization ( $P_s$ ) and depolarizing field ( $E_d$ ).....	10
Figure 2.5	Ferroelectric polarization hysteresis loop. Hexagon represents schematically repartition of two polarization states.....	10
Figure 2.6	Molecular structure of P(VDF-TrFE).....	11
Figure 2.7	Experimental capacitance device structure.....	12
Figure 2.8	Experimental polarization hysteresis.....	12
Figure 2.9	Experimental small-signal C-V curve.....	12
Figure 2.10	Applied voltage signal for PUND measurement.....	13
Figure 2.11	Experimental and SILVACO simulated hysteresis curves using mathematical expression from S. L. Miller <i>et al.</i> .....	15
Figure 2.12	Experimental and MATLAB simulated hysteresis curves using mathematical expression from S. L. Miller <i>et al.</i> .....	16
Figure 2.13	Experimental and MATLAB simulated hysteresis curve using Landau theory for monocrystalline ferroelectric.....	19
Figure 2.14	Experimental and MATLAB simulated hysteresis curve using J. Yu <i>et al.</i> model.....	22



Figure 2.15	Experimental and MATLAB simulated polarization hysteresis using Landau free energy expression by Y. L. Wang <i>et al.</i> .....	25
Figure 2.16	Experimental and MATLAB simulated polarization hysteresis using modified Y. L. Wang <i>et al.</i> model.....	26
Figure 3.1	Experimental and MATLAB simulated polarization hysteresis of ferroelectric by calculating the constants $\beta_1$ and $\beta_2$ .....	31
Figure 3.2	Unit Step function.....	32
Figure 3.3	Experimental and MATLAB simulated polarization hysteresis of ferroelectric by using new practical model with Three-point fit.....	33
Figure 3.4	Experimental and MATLAB simulated polarization hysteresis of ferroelectric by using new practical model with four-point fit.....	37
Figure 4.1	MATLAB simulated large signal C-V curve using modified Miller <i>et al.</i> model.....	41
Figure 4.2	Silvaco simulated large signal C-V curve using modified Miller <i>et al.</i> model.....	41
Figure 4.3	Overlay of analytic large-signal and experimental small-signal capacitance.....	43
Figure 4.4	Large-signal capacitance using point to point numerical derivative....	44
Figure 4.5	Overlay of large-signal capacitance produced using analytical approach and numerical derivative approach by skipping every three points.....	45
Figure 4.6	Circuit model of a ferroelectric capacitor.....	46
Figure 4.7	Experimental and MATLAB simulated small-signal capacitance curve.....	48
Figure D.1	Experimental and MATLAB simulated polarization hysteresis of ferroelectric by using new practical model with four-point fit on negative going curve.....	65

## **Abstract**

# **MODELING POLARIZATION AND CAPACITANCE HYSTERESIS OF FERROELECTRIC CAPACITORS**

Bikash Shrestha

Thesis Chair: Ron J. Pieper, Ph. D.

The University of Texas at Tyler  
May 2012

A simulation based comparative study of the polarization hysteresis of the ferroelectric capacitor using various ferroelectric models is presented. A 2-dimensional finite element device-level model was implemented using SILVACO's ATLAS device simulator to generate the polarization hysteresis characteristics for Au/Poly(vinylidene fluoride-trifluoroethylene)/Au metal-insulator-metal (MIM) device. Landau free energy expression for electric field in terms of polarization is also implemented in MATLAB to produce the polarization hysteresis curves of monocrystalline and polycrystalline ferroelectrics. The main drawback of previous models was their inability to predict polarization saturation at the same electric field limits as compared with measurements taken from a recently fabricated ferroelectric capacitor. A new model for ferroelectric polarization hysteresis based on curve fitting algorithm is derived that forces the polarization to be saturated at the desired electric field. The MATLAB simulation of this model and the experimental hysteresis is compared which shows an excellent level of agreement.

The capacitance hysteresis of the ferroelectric capacitor is also analyzed using the MATLAB simulation. The new polarization hysteresis model that uses four-point fit method is used to derive the mathematical expression for large-signal capacitance. Landau-Khalatnikov kinetic equation is used for deriving mathematical expression for small-signal capacitance. The capacitance simulation results agreed fairly well with physical measurements from a Au-P(VDF-TrFE)-Au capacitor.

# **Chapter 1**

## **Introduction**

### **1.1 Ferroelectricity: Introduction, History and Applications**

The ever growing computing and communication technology demands for further decrease in device size with larger data storage capacity and higher speed [1]. The energy efficiency, convenience, affordability and reliability are the major qualities that are needed in the next generation computing and communication devices [2]. In recent years, ferroelectric material is being viewed as the future of computing because of its application in manufacturing fast, compact and low power non-volatile memory devices [3]. Beside memory applications, ferroelectrics also show a vast potential in different applications such as sensors, RF devices, actuators [4], thermistors and transducers [5]. Its potential for memory applications was realized after its discovery in 1920 by Valasek in Rochelle salt [6] but progress has long been hampered because of the difficulties in material processing and integration [1]. The research interest in ferroelectric memory grew significantly since the early 1950s but the requirement of large biases for switching the polarization made this application impractical. The feasibility of ferroelectric memory was rendered in early 1990s when significant advances were made in sol-gel thin film synthesis with coercive biases well below 10V. Since then ferroelectric random access memory (FeRAM) with the advantage of non-volatility and ferroelectric transistors are being fabricated as ferroelectric memory devices. [7]. Ferroelectricity was not in common use before early 1940s because Rochelle salt was the only known ferroelectric material and no theoretical interpretation of the phenomenon was given because of the complex and unknown crystal structure of Rochelle salt [6]. The discovery of ferroelectricity in mixed oxides having perovskite crystalline structure in early 1940s was the turning point in the history of ferroelectricity [5]. Because of the simple crystalline structure and

practical utility (chemical and mechanically very stable) of perovskite oxides, it attained a lot of scientific curiosity that led to the theoretical progress at the microscopic level [6]. During the period 1950 to 1960, research into ferroelectrics gained so much attraction that many new ferroelectrics were discovered. That's why this period is considered as the 'period of proliferation' in the ferroelectric history [5]. Early researches in the field of ferroelectricity explored the ferroelectric crystals as material for ultrasonic transducers in SONAR systems and medical ultrasound imaging. In this period, the development in single crystal growth and broad study of ferroelectricity made possible the application of ferroelectric materials in electrooptical systems and photothermal imaging. The advancement in thin film synthesis and microfabrication in recent decades has resulted in the use of ferroelectrics in microelectromechanical systems, nanoscale optics, nanophotonics and plasmonics [7].

Ferroelectricity is a phenomenon in which spontaneous electric polarization of the material can be reversed or switched by applying an external electric field. A ferroelectric crystal has two or more orientation states that can be shifted from one to another without destroying the crystal by applying an external electric field. According to the geometry of the crystals, they are classified into seven systems. These systems are further divided into 32 crystal classes (point groups) depending on their symmetry with respect to a point. Eleven of them have center of symmetry and the remaining 21 belong to non-centric crystal classes [6]. Among them, 10 crystal classes possess a unique polar axis and these classes are called polar crystal point group. Ferroelectric materials belong to this group [8]. However, every polar crystal (for example wurtzite-structure insulator) is not ferroelectric because for ferroelectricity the switching of polarization with an applied electric field should be possible [9]. The crystal structure of any two of the orientation states of ferroelectrics are identical but differ in the direction of spontaneous electric polarization [6]. Spontaneous polarization is produced because of the polar displacement of the atoms in a unit cell of the ferroelectric crystal [9]. A dipole is formed when two equal and opposite charges are separated by certain distance. The product of the point charge and the separating distance is called the dipole moment. The number of dipoles per unit volume is called polarization. Polarization does not mean charging of the

material. The polarized material is electrically neutral. A unit cell of a material possesses a dipole moment when the center of positively charged ions and center of negatively charged ions do not coincide. [10]. The material possesses the ferroelectricity only when the overall dipole moments within the material do not cancel out completely. The dipole moments of the amorphous material are randomly orientated and cancel each other, whereas they do not cancel each other in the case of asymmetric crystal. So only the asymmetric crystals can possess the ferroelectricity [11]. A ferroelectric material possesses electric polarization below certain temperature known as Curie temperature ( $T_C$ ) [8]. Above this temperature the center of the positive and negative charge of a unit cell of the material coincide with each other and the material can no longer possess ferroelectricity. This phase of the material is called paraelectric phase. The spontaneous electric polarization can also be affected by the temperature and the external stress. The dependence of spontaneous polarization on temperature is pyroelectricity [12] and the production of electric polarization by the application of stress is called piezoelectricity [6]. The relation between pyroelectricity, piezoelectricity and ferroelectricity is such that all the ferroelectric materials are pyroelectric and all the pyroelectric materials are piezoelectric [13].

## 1.2 Literature Review

The application of ferroelectrics as a memory has become a popular research field in recent years because it performs as a read only memory (ROM) even with the circuit configuration similar to that of dynamic random access memory (DRAM) [14]. This property of non-volatility in ferroelectric capacitors and transistors is attributed to the formation of polarization-Electric field (P-E) hysteresis loop. There have been many efforts to model a ferroelectric capacitor but there is still not a universal, accurate and physical based model that could describe the material behavior of ferroelectric capacitor [15]. A quantitative model for the circuit containing non-ideal ferroelectric capacitor was given by Miller *et al.* The model considers the ferroelectric capacitor as a stack of switching ferroelectric layer and non-switching dielectric layers. They chose the hyperbolic tangent function to relate polarization and electric field and derived a

mathematical model for producing hysteresis loop. The model also satisfies the formation of unsaturated hysteresis loop when the applied field is not enough to drive the polarization into saturation [16]. P. Gang *et al.* developed a phenomenological model based on the physical behavior of polarization reversal. This model works well for both saturated and unsaturated hysteresis loops. This model also can well describe the polarization for any arbitrary conditions [15]. A compact model based on dipole switching theory which can well describe both saturated and unsaturated hysteresis loop is derived by J. Yu *et al.* [17]. A curve fitting algorithm for modeling polarization hysteresis is given by C. Fu *et al.* that divides one branch of the hysteresis curve into three different domain curves with nine unknown constants and extracts the polarization values from the measured hysteresis curve to produce an analytic representation [18]. C. J. Brennan gave a mathematical model for producing hysteresis loop of ferroelectric thin film capacitors based on physical principles, not a curve fitting algorithm [19]. Brennan derived the expression for hysteresis of mono-crystalline ferroelectrics from the Landau free energy considerations. He also gave the derivation for the hysteresis of polycrystalline ferroelectrics considering the spatial orientation and structural phase of the crystallites. Y. L. Wang *et al.* used Landau free energy theory for modeling hysteresis of polycrystalline ferroelectrics and followed the curve fitting approach [20]. All the models mentioned above have immense contribution in the field of ferroelectric by bringing up different perspective for modeling polarization hysteresis but these models did not produce sufficient level of agreement with our experimental hysteresis as described in detail in Chapter 2. The main drawback of these models was their inability to predict polarization saturation at the same electric field limits for which the experimental device was saturating. In our recent work, a new mathematical model for generating polarization hysteresis based on curve fitting algorithm is derived that forces the polarization curve to saturation level at desired electric field [21].

### 1.3 Objective

The polarization hysteresis is a peculiar property of ferroelectrics that can be utilized to devise a storage element in integrated nonvolatile memory application [2]. In

order for a ferroelectric capacitor to work as a memory device in integrated circuits, an accurate model that could describe the behavior of the ferroelectric capacitor should be created. The main objective of our thesis is to create such models that could describe the formation of polarization and capacitance hysteresis in a ferroelectric capacitor. In this thesis, a ferroelectric capacitor based on P(VDF-TrFE) is considered for testing the simulation results from different existing models as well as from our new models. The comparison of the experimental polarization hysteresis and simulated polarization hysteresis from different existing models shows a discrepancy between them. The main discrepancies are in the saturation region and in the vicinity of the coercive field of the hysteresis loop. This demands for the development of a new practical model for the polarization hysteresis of a ferroelectric capacitor which can satisfy the experimental hysteresis curve; so a new mathematical polarization hysteresis model is developed using the curve fitting algorithm. Our new mathematical model is based on the Y. L. Wang *et al.* model [20]. The first objective is to develop a mathematical formula for calculating the constants  $\beta_1$  and  $\beta_2$  which values were chosen by trail and error to fit the experimental hysteresis data within context of Y. L. Wang *et al.* model. The simulation of polarization hysteresis using this model does not agree with the experimental hysteresis adequately; so further modification is done in the model using both three-point fit and four-point fit approaches. Considering the four points in a branch of the hysteresis curve, the model gives an excellent level of agreement with experimental polarization hysteresis and the mathematical complexity is still in the satisfactory level.

Another objective of this thesis work is to be able to model the capacitance hysteresis by using polarization hysteresis. The model of S. L. Miller *et al.* polarization hysteresis is modified to generate large-signal capacitance and simulated using Silvaco's Atlas device simulator and MATLAB. Our new model for polarization that uses four-point fit approach is also applied to generate the mathematical model for large-signal capacitance and implemented in MATLAB. Since the experimental capacitance hysteresis is small-signal capacitance, no comparison is done between experimental capacitance hysteresis and simulation results from large-signal capacitance models. Finally, a model for small-signal capacitance which considers the Landau-Khalatnikov

dynamic equation is simulated using MATLAB and the comparison with experimental capacitance hysteresis shows a fair level of agreement.

#### **1.4 Thesis Organization**

The theory of ferroelectrics and the formation of polarization hysteresis are discussed in Chapter 2 considering the perovskite oxide as a ferroelectric. A brief description about our experimental ferroelectric capacitor and our experimental ferroelectric material P(VDF-TrFE) are also given. The most sections of the Chapter 2 describe the existing models for polarization hysteresis, their implementation in simulation tools and comparison of the simulation results with experimental polarization hysteresis. In Chapter 3, new mathematical models for predicting polarization hysteresis and the comparison of simulation results with experimental hysteresis are presented. These models include the model based on predicting coefficients  $\beta_1$  and  $\beta_2$  of Y. L. Wang *et al.* model, the model with the Three-point fit approach and the model with the four-point fit approach. Chapter 4 discusses the capacitance modeling. Large-signal capacitance models using modified Miller *et al.* model and using four-point fit model are described and simulated in MATLAB. This chapter also discusses about small-signal capacitance model and the comparison of simulated curve with experimental one. Finally in Chapter 5, the thesis is concluded summarizing the contributions of this thesis work and some suggestions for future work.



## Chapter 2

### Background Study

#### 2.1 Perovskite Oxide and Ferroelectric Theory

Since perovskite oxides are widely studied ferroelectrics, the ferroelectricity phenomenon and its related terms are discussed considering perovskite oxide with general formula  $ABO_3$  as an example. A and B each represents a cation element or a mixture of the cations and O stands for an oxygen element. It has a simple cubic lattice structure with 5 atoms per unit cell. There are two ways of viewing a unit cell of the perovskite crystal as shown in the Figure 2.1 [9].

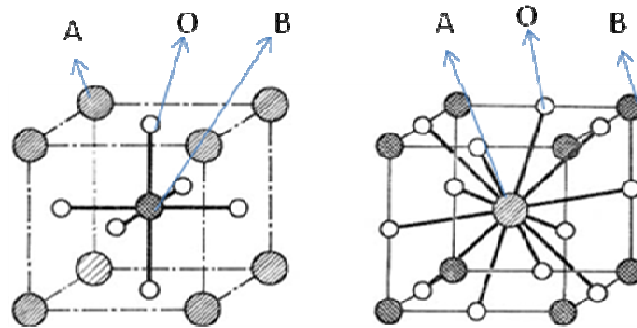


Figure 2.1: Two different views of a unit cell of a perovskite oxide [9].

If atom A is considered at the corner of the cube, atom B will be at the center and Oxygen will be at the center of each face. If atom B is taken at the corner, atom A will be at the center and Oxygen at the midpoint of each edge [9]. The crystal structure is exactly cubic with center of symmetry above the Curie temperature ( $T_C$ ) where it loses the ferroelectric properties [23]. Below the Curie temperature, the macroscopic strain causes

the electrostrictive distortion involving displacement of the cations relative to the anions in the unit cell that produces the polarization [8, 9, 24]. The crystal undergoes tetragonal, orthorhombic or rhombohedral ferroelectric phase transition depending on the direction of polarization and temperature conditions [8]. Fig 2.2 shows the generation of polarization in  $\text{BaTiO}_3$  unit cell because of the shifting of Ba and Ti sub-lattices relative to the negatively charged Oxygen.

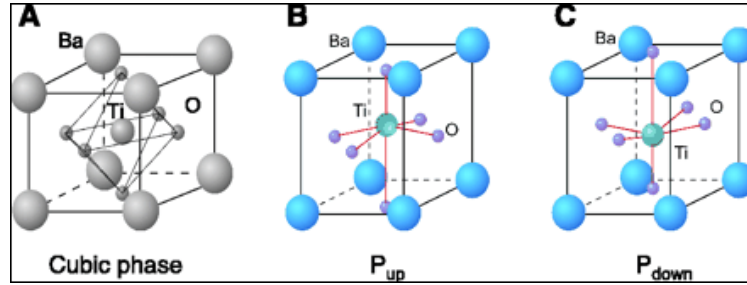


Figure 2.2: Generation of polarization in a  $\text{BaTiO}_3$  unit cell [9].

The direction of polarization within a crystal is not uniformly aligned in a same direction; it depends on the electrical and mechanical boundary conditions imposed on the crystal sample [13]. The region of the crystal where the uniformly orientated spontaneous polarization lies is called ferroelectric domain, and the region between the two domains is called the domain wall as shown in the Figure 2.3. Ferroelectric domains are formed to minimize the electrostatic energy of the depolarizing field and elastic energy associated with the mechanical conditions to which the ferroelectric crystal is subjected [13]. The depolarization field is one of the factors controlling ferroelectric phase stability [7]. It is produced because of the non-homogeneities in the spontaneous polarization distribution [13, 25]. Surface charges formed by spontaneous polarization gives rise to an electric field, called depolarizing field ( $E_d$ ) which is oriented opposite to the spontaneous polarization as shown in the Figure 2.4 [13]. The formation mechanism of domains and domain walls results in hysteresis curve which shows relationship between applied electric field and electric polarization [23, 26]. The application of external field produces force which exerts pressure on the domain walls that tends to reorient the domains in the direction of applied electric field [13, 26]. When all the domains in a crystal are orientated only in one direction, it is said to be in single-domain

or mono-domain state. This process of reorienting domains and producing single domain crystal is called poling [13]. When small alternating field is applied to the natural multi-domain ferroelectric crystal, polarization increases linearly with the field amplitude, corresponding to line segment AB in the hysteresis curve as shown in Figure 2.5. As the field increases, polarization of domains starts to switch nonlinearly along the direction of the field as given by the line segment BC in the hysteresis curve. C is the point where all the domains of the crystal are oriented in one direction and the corresponding polarization value refers to spontaneous polarization ( $P_S$ ). Further increase in the external applied field beyond this point again gives a linear relationship with polarization. When the external applied electric field starts decreasing, some of the domains switch back but the crystal still possesses some polarization value at zero applied fields which is called remnant polarization ( $P_R$ ) [13]. The polarization is brought back to zero by applying negative electric field equivalent to the portion AF in the hysteresis curve. This electric field corresponding to zero polarization is called coercive field ( $E_C$ ). Further decrease in field causes the domains to completely switch in the opposite direction. Reversing the field again and going back to positive saturation point completes the formation of the hysteresis loop [13, 23]. An ideal hysteresis loop is symmetrical on both X and Y axes, so the magnitude of positive and negative  $P_S$ ,  $P_R$  and  $E_C$  are equal. The shape of the hysteresis loop may depend upon the thickness of the crystal, presence of charged defects, mechanical stresses, preparation conditions and thermal treatment [13, 26]. The variation of polarization (P) with electric field (E) in ferroelectric hysteresis curve is similar to the variation of magnetization (M) of ferromagnets with magnetizing field (H) [11]. Consequently the term “Ferroelectricity” originates from the analogy to “Ferromagnetism”.

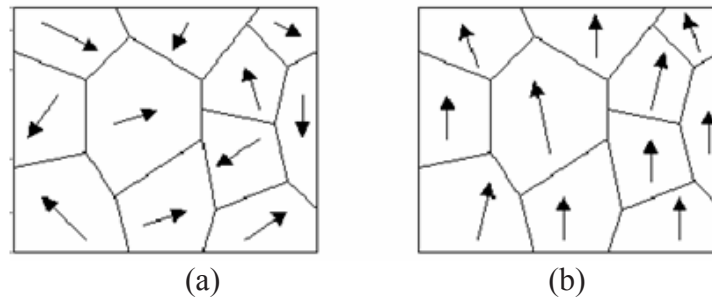


Figure 2.3: Domains and domain walls (a) before poling and (b) after poling [13].

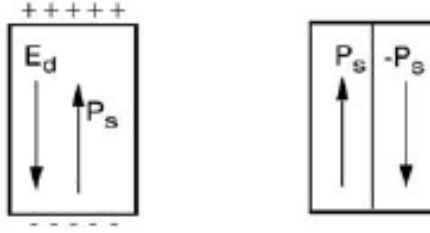


Figure 2.4: Spontaneous polarization ( $P_s$ ) and depolarizing field ( $E_d$ ) [13].

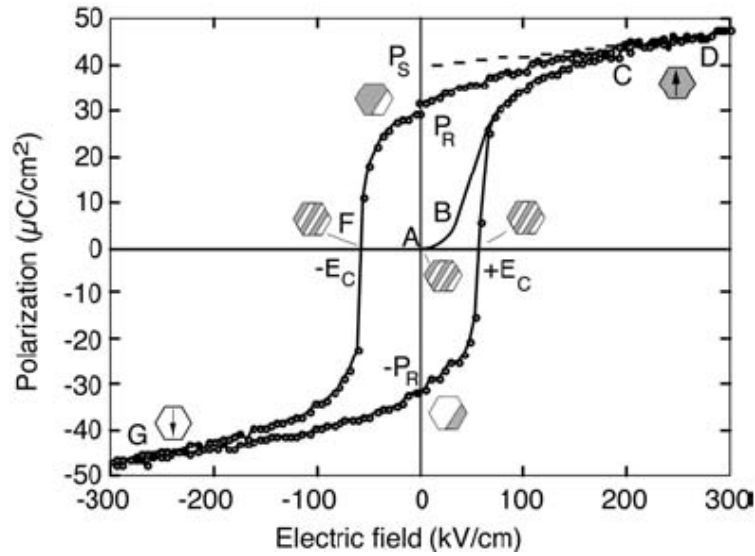


Figure 2.5: Ferroelectric polarization hysteresis loop. Hexagon represents schematically repartition of two polarization states. [13].

## 2.2 P(VDF-TrFE)

Organic ferroelectrics have gained much attention over last several years because of easy and simple device fabrication methods, chemical stability, mechanical flexibility, light weight and low cost [27, 28, 29]. Among many organic ferroelectrics, polyvinylidene fluoride copolymer with trifluoroethylene (P(VDF-TrFE)) is a promising candidate in the most of the ferroelectric applications because of its advantageous properties such as large remnant polarization, good thermal stability, absence of size effects, short switching time and compatibility with many organic molecules and biomolecules [11, 29, 30, 31, 32]. It demonstrates the polarization switching in nanometer scale making it suitable ferroelectric material for the applications in

nanotechnology and microelectronics [31]. The molecular formula of PVDF is  $(\text{CH}_2\text{CF}_2)_n$  and its copolymer P(VDF-TrFE) is  $(\text{CH}_2\text{CF}_2)_n-(\text{CHF}\text{CF}_2)_m$  [11]. The molecular structure of P(VDF-TrFE) is shown in Figure 2.6. The Fluorine atom in PVDF has higher electron affinity than Hydrogen, so the electrons are shifted more towards Fluorine forming dipoles. PVDF films processed directly from melt or from a solution are not ferroelectric because the dipole moments in such crystal cancel with each other. Additional work such as stretching the copolymer to change the crystal conformation is required to make these films ferroelectric. Another way to make these films ferroelectric is to make PVDF copolymer with TrFE. The presence of additional Fluorine atom in TrFE changes crystal conformation that aligns the direction of the dipole moment [11].

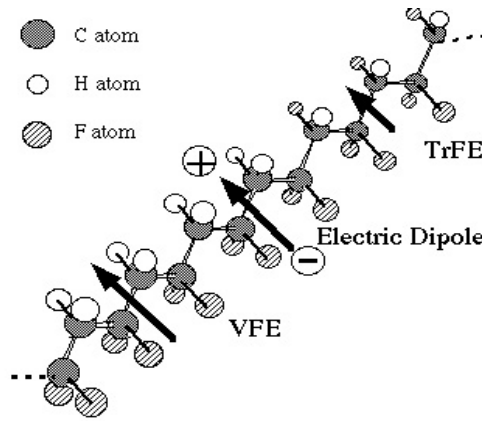


Figure 2.6: Molecular structure of P(VDF-TrFE) [11].

## 2.3 Experimental Ferroelectric Capacitor

The device structure of the experimental ferroelectric capacitor is given in the Figure 2.7. Gold with the work function=5.1 eV is used as the electrodes and P(VDF-TrFE) copolymer with 70/30 mol ratio is used as ferroelectric insulator. The copolymer P(VDF-TrFE) of thickness 210 nm is annealed at 133 °C for 2 hours in a vacuum oven [33]. The area of the device is 0.0005 cm<sup>2</sup>. The electrical performance of the device is characterized using polarization (P) - voltage (V) and capacitance (C) - voltage (V) characteristics as shown in the Figure 2.8 and Figure 2.9 respectively. The measurement device RT66B from Radiant Technology is used to measure the P-V characteristics where as HP4284 from Agilent is used to measure the C-V characteristics. These experimental

curves shown in Figure 2.8 and Figure 2.9 are taken from D. Mao et al. corresponding to 133 °C annealing temperature and 210 nm P(VDF-TrFE) thickness [33].

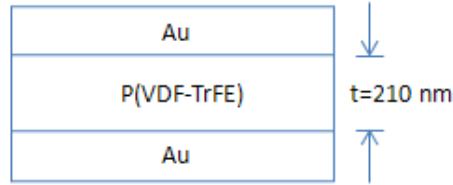


Figure 2.7: Experimental capacitance device structure.

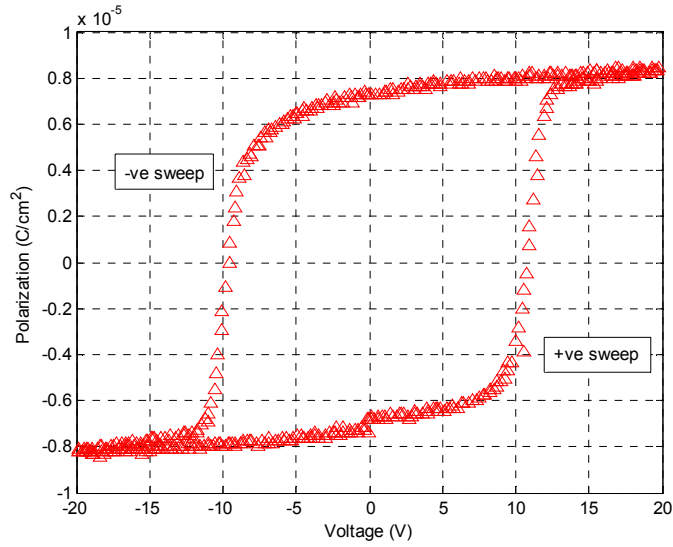


Figure 2.8: Experimental polarization hysteresis.

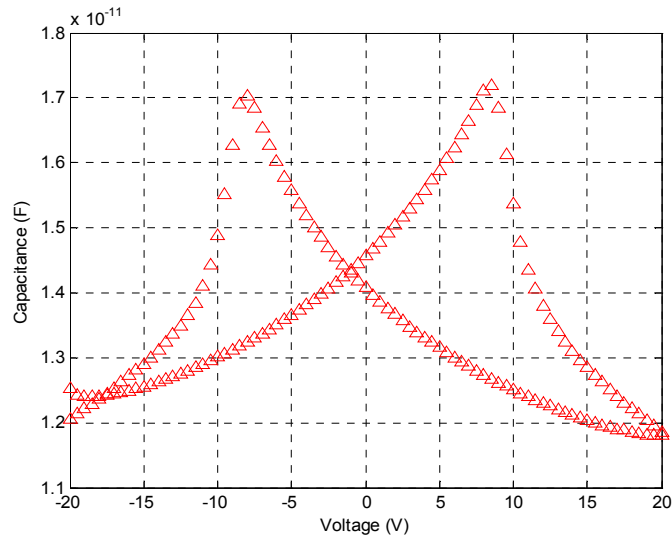


Figure 2.9: Experimental small-signal C-V curve.

Ferroelectric polarization was measured using standard ferroelectric memory characterization method known as positive up negative down (PUND) method [34]. In this method, the pulse shown in Figure 2.10 is applied to the ferroelectric capacitor. The first negative pulse initializes the capacitor into negative polarization. The second pulse measures the charge switched from negative remnant polarization state to positive maximum polarization state denoted by  $P_{sw}$ , corresponding to the integration of current in switching transient. The third pulse is used to measure non-switched charge from positive maximum polarization to the positive remnant polarization state denoted by  $P_{ns}$ , equivalent to the integration of current when the capacitor is switched at the same polarity. The fourth and the fifth pulses measure both  $P_{sw}$  and  $P_{ns}$  in the opposite direction [34]. The values of  $P_S$ ,  $P_R$  and  $E_C$  are extracted from the polarization hysteresis. The positive sweep curve and negative sweep curve are not symmetric; so the extracted values of  $P_S$ ,  $P_R$  and  $E_C$  for two different sweeps are different as tabulated in Table 2.1.

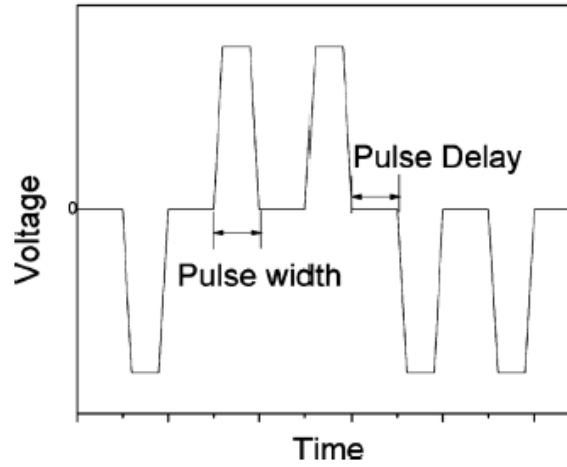


Figure 2.10: Applied voltage signal for PUND measurement [34].

Table 2.1: Extracted values of the parameters from experimental polarization hysteresis.

Parameters	Experimental (+ve sweep)	Experimental (-ve sweep)	Experimental (average)
$E_C$	$0.5145 \times 10^6 \text{ V/cm}$	$-0.4549 \times 10^6 \text{ V/cm}$	$0.4847 \times 10^6 \text{ V/cm}$
$P_R$	$-7.41 \times 10^{-6} \text{ C/cm}^2$	$7.29 \times 10^{-6} \text{ C/cm}^2$	$7.35 \times 10^{-6} \text{ C/cm}^2$
$P_S$	$8.461 \times 10^{-6} \text{ C/cm}^2$	$-8.2274 \times 10^{-6} \text{ C/cm}^2$	$8.34 \times 10^{-6} \text{ C/cm}^2$

## 2.4 Polarization Hysteresis Modeling

Accurate modeling of a ferroelectric capacitor has always been a difficult task. This is because the P-V and C-V characteristics of ferroelectric capacitor depend not only on the present position but also on its history [19, 35]. There have been many attempts to model ferroelectric capacitors as mentioned in Chapter 1. In this chapter, we discuss some of those ferroelectric hysteresis models and implement to satisfy our experimental hysteresis.

### 2.4.1 S. L. Miller *et al.* Model [16]

S. L. Miller *et al.* developed a mathematical model for characterizing the circuit behavior containing non-ideal ferroelectric capacitor. This model is used in the current finite element device simulator Atlas from Silvaco International [36]. They viewed a ferroelectric capacitor as the stack of switching ferroelectric layer and non-switching dielectric layers. The non-switching dielectric layers are generated due to the physical and electrical interaction of ferroelectric with electrodes. These layers bring the non-ideality in the ferroelectric capacitor. These layers are considered adjacent to each electrode. There is a ferroelectric switching layer between two non-switching dielectric layers where dipole polarization is function of electric field and previous history. When applied electric field ( $E$ ) is varied between two same but opposite values enough to align all dipoles in one direction, the dipole polarization ( $P_d$ ) approaches the value of the spontaneous polarization ( $P_s$ ). It also considers that dipole polarization is zero where the electric field equals to the coercive field ( $E_C$ ) and it has some value at zero fields which is remnant polarization ( $P_R$ ). The two branches of saturated switching dipole polarization curve is assumed to be symmetric which is expressed by,

$$P_d^-(E) = -P_d^+(-E) \quad (2.1)$$

where,  $P_d^-(E)$  and  $P_d^+(E)$  are negative and positive going polarization branches of the hysteresis loop respectively. The behavior of dipole switching as a function of electric field is given by hyperbolic tangent function. This mathematical function satisfies the



physical requirements for hysteresis formation and has convenient mathematical properties. So the relation between  $P_d^+(E)$  and electric field ( $E$ ) is given by,

$$P_d^+(E) = P_s \tanh \left[ \frac{(E - E_c)}{2\delta} \right] \quad (2.2)$$

The expression for  $\delta$  is predicted using the relation,  $P_d^+(0) = -P_R$ . The detail mathematical derivation is given in Appendix A.

$$\delta = E_c \left[ \log \left( \frac{1 + P_R / P_s}{1 - P_R / P_s} \right) \right]^{-1} \quad (2.3)$$

The electric field and voltage are related as,

$$E = V/t \quad (2.4)$$

where “t” is the thickness of the ferroelectric material as shown in Figure 2.7. The negative branch of saturated switching dipole polarization is calculated by using (2.1).

This mathematical model is implemented within Silvaco’s ATLAS device simulator for ferroelectrics and MATLAB and compared with experimental polarization hysteresis as shown in Figure 2.11 and Figure 2.12. The corresponding values of parameters for the simulation and the experimental values are listed on Table 2.2.

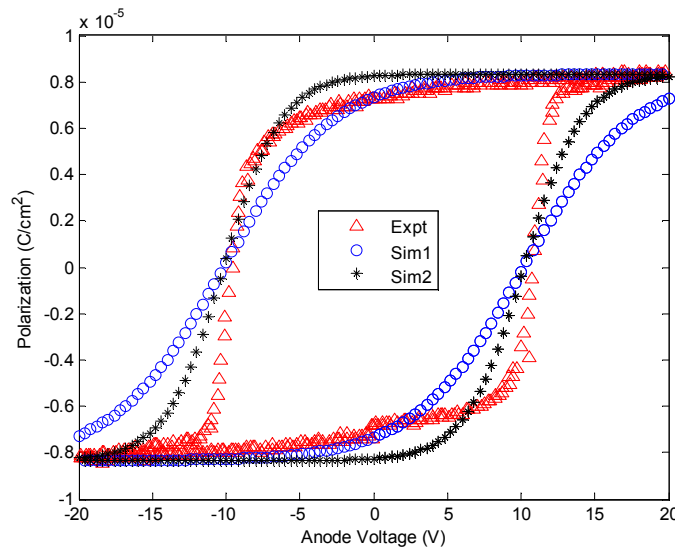


Figure 2.11: Experimental and SILVACO simulated hysteresis curves using mathematical expression from S. L. Miller *et al.*

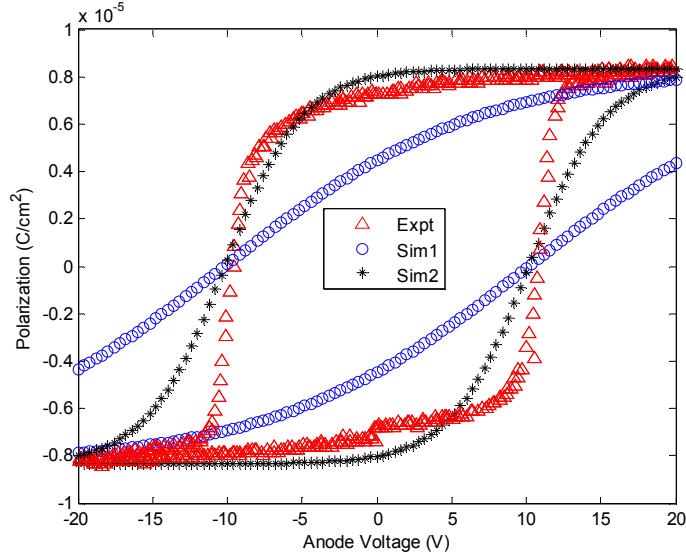


Figure 2.12: Experimental and MATLAB simulated hysteresis curves using mathematical expression from S. L. Miller *et al.*

Table 2.2: Experimental values and corresponding Silvaco and MATLAB simulation parameters for model by S. L. Miller *et al.*

Parameters	Experimental	Silvaco		MATLAB	
		Sim1	Sim2	Sim1	Sim2
$E_C$ (V/cm)	$4.847 \times 10^5$	$4.847 \times 10^5$	$4.847 \times 10^5$	$4.847 \times 10^5$	$4.847 \times 10^5$
$P_R$ (C/cm <sup>2</sup> )	$7.35 \times 10^{-6}$	$7.35 \times 10^{-6}$	$8.25 \times 10^{-6}$	$7.35 \times 10^{-6}$	$8.338 \times 10^{-6}$
$P_S$ (C/cm <sup>2</sup> )	$8.34 \times 10^{-6}$	$8.34 \times 10^{-6}$	$8.34 \times 10^{-6}$	$8.34 \times 10^{-6}$	$8.34 \times 10^{-6}$
permittivity	9	9	9	9	9

The simulation curves “Sim1” for both Silvaco and MATLAB simulations is generated using exactly the same parameter values from the experiment. This simulation curve did not reach the saturation level as experimental hysteresis. By adjusting the remnant polarization ( $P_R$ ) to be slightly higher than experimental data as shown in Table 2.2, the “Sim2” model curves for both Silvaco and MATLAB simulations go into saturation faster. Although agreement between experiment and “Sim2” model is better in the polarization saturation, the discrepancy for remnant polarization at  $E=0$  is apparent in Figure 2.11 and Figure 2.12.

### 2.4.2 Landau Free Energy Model for Monocrystalline Ferroelectrics [19]

Landau theory is symmetry based analysis that describes the system's equilibrium behavior near the phase transition [9]. A ferroelectric system cannot change smoothly between ferroelectric and paraelectric phases because the two phases are symmetrically distinct. Landau theory characterizes the phase transition in terms of an order parameter which is a physical entity that is zero at high symmetry and has a finite value when symmetry is lowered. The polarization ( $P$ ) is the order parameter for paraelectric-ferroelectric phase transition. The free energy  $F(P)$  whose minimum determines the equilibrium state of the system, can be expanded as a power series of order parameter in the vicinity of the phase transition [9]. The polarization hysteretic behavior of monocrystalline ferroelectric is derived from the Landau-Devonshire expression for free energy  $F(P)$  in terms of polarization which is given as [19],

$$F(P) = F_0 - \frac{\alpha}{2}P^2 + \frac{\beta}{4}P^4 + \dots \quad (2.5)$$

where  $\alpha$  and  $\beta$  are Landau coefficients and  $F_0$  is the free energy in paraelectric state. Taking the derivative of above equation and neglecting the higher order terms, we get the following expression for the electric field ( $E$ ) as a function of polarization [19].

$$\frac{\partial F}{\partial P} = E = -\alpha P + \beta P^3 \quad \text{or} \quad \beta P^3 - \alpha P - E = 0 \quad (2.6)$$

The zeros of this function gives value of spontaneous polarization and the value of  $E$  at local minimum and maximum gives the value of coercive field [19]. Landau coefficients can be calculated from the experimental measured values of  $P_s$  and  $E_c$  using the formula given below. The detail mathematical derivation for finding  $\alpha$  and  $\beta$  is given in the Appendix B.

$$\alpha = \beta P_s^2 \quad (2.7)$$

$$\beta = -\frac{3\sqrt{3}E_c}{2P_s^3} \quad (2.8)$$

The value of polarization for each value of electric field ( $E$ ) is calculated by finding the cubic roots of (2.6) as follows [19].

$$P_1(E) = S + T \quad (2.9)$$

$$P_2(E) = -\frac{1}{2}(S + T) + \frac{1}{2}j\sqrt{3}(S - T) \quad (2.10)$$

$$P_3(E) = -\frac{1}{2}(S + T) - \frac{1}{2}j\sqrt{3}(S - T) \quad (2.11)$$

where,  $j = \sqrt{-1}$ ,

$$S = \sqrt[3]{R + \sqrt{Q^3 + R^2}} \quad (2.12)$$

$$T = \sqrt[3]{R - \sqrt{Q^3 + R^2}} \quad (2.13)$$

Equations (2.9) to (2.13) represent the reported rules needed to solve a cubic equation [37]. Because the coefficient ' $a_1$ ' of  $E^2$  in (2.6) is zero, the  $R$  and  $Q$  terms were expressed as [19],

$$R = \frac{E}{2 * \beta} \quad (2.14)$$

$$Q = -\frac{\alpha}{3 * \beta} \quad (2.15)$$

There are three values of polarization for each value electric field ( $E$ ) as given by (2.9) (2.10) and (2.11). One polarization value for each value of electric field ( $E$ ) is determined by selecting a real valued root which is closest in the value to the previous polarization point [19].

This mathematical model is implemented in MATLAB and compared with experimental polarization hysteresis as shown in Figure 2.13. The values of the parameters used for the simulation are tabulated in Table 2.3. The parameter  $P_R$  is not needed for this simulation. The calculated value of  $\alpha$  and  $\beta$  are also given in Table 2.3. Simulation hysteresis shows good level of agreement with experimental hysteresis in saturation region for much lower value of  $P_S$  than experimental value as given in above

table. The simulation hysteresis curve also shows a sudden switching of the polarization at coercive field as shown in Figure 2.13. This could be adjusted by considering higher order terms of Landau-Devonshire expression or by using a more sophisticated molecular force model [19].

Table 2.3: Experimental and MATLAB simulation parameters for model using Landau free energy theory for monocrystalline ferroelectric.

Parameters	Experimental	MATLAB
$E_C$	$0.4847 \times 10^6$ V/cm	$0.4847 \times 10^6$ V/cm
$P_S$	$8.34 \times 10^{-6}$ C/cm <sup>2</sup>	$6.8 \times 10^{-6}$ C/cm <sup>2</sup>
$\alpha$	N/A	$1.85 \times 10^{11}$ cm/F
$\beta$	N/A	$4.0 \times 10^{21}$ cm <sup>5</sup> /F.C <sup>2</sup>

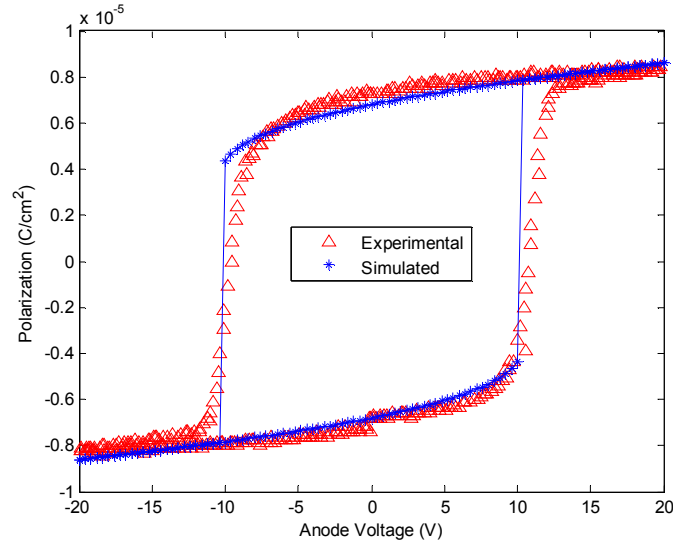


Figure 2.13: Experimental and MATLAB simulated hysteresis curve using Landau theory for monocrystalline ferroelectric.

#### 2.4.3 J. Yu *et al.* Model [17]

Modeling of a ferroelectric capacitor can be categorized into two areas; behavioral models and physical models. Behavioral models characterize the ferroelectric capacitor with the circuit point of view which doesn't need the detailed knowledge of the

ferroelectric theory, so these models cannot explain the material behavior of the ferroelectric capacitor [17, 35]. However, physical models consider the theory of ferroelectrics and hence explain the physical character of the ferroelectric capacitor. J. Yu *et al.* developed a physical model for characterizing the polarization hysteresis based on dipole switching theory. This model also considers the ferroelectric capacitor as a stack of two non-switching dielectric layers and a switching dielectric layer in between as assumed by Miller *et al.* The total polarization of a ferroelectric capacitor is the sum of polarization due to switching dielectric and polarization contributed by non-switching dielectric.

$$P = P_f + P_d \quad (2.15)$$

The polarization due to non-switching dielectric  $P_d$  has linear relationship with applied field  $E$ .

$$P_d = \alpha E \quad (2.16)$$

where  $\alpha$  is a constant determined by experiment. The relation between polarization due to switching dielectric (ferroelectric polarization) and applied field is determined by the dipole switching theory which is given by,

$$P_f = P_m - (P_m + P_{sat}) \left\{ \frac{1}{\pi} \tan^{-1} [-\delta_D (E_C - E)] + \frac{1}{2} \right\} \quad (2.17)$$

So the total polarization is given by,

$$P = P_m - (P_m + P_{sat}) \left\{ \frac{1}{\pi} \tan^{-1} [-\delta_D (E_C - E)] + \frac{1}{2} \right\} + \alpha E \quad (2.18)$$

The expressions of polarization for positive field sweep and for negative field sweep can be written separately as follows.

$$P_U = P_m^+ - (P_m^+ + P_{sat}^+) \left\{ \frac{1}{\pi} \tan^{-1} [-\delta^+ (E_C^+ - E)] + \frac{1}{2} \right\} + \alpha^+ E \quad (2.19)$$

$$P_D = P_m^- - (P_m^- + P_{sat}^-) \left\{ \frac{1}{\pi} \tan^{-1} [-\delta^- (E_C^- - E)] + \frac{1}{2} \right\} + \alpha^- E \quad (2.20)$$

where  $P_m$ ,  $P_{sat}$  and  $E_C$  are polarization for maximum electric field, saturation polarization and coercive field respectively. The sign on the superscript gives the positive or negative value of them accordingly.

The constants  $\alpha^+$ ,  $\alpha^-$ ,  $\delta^+$  and  $\delta^-$  can be calculated using following relations. The detail mathematical derivation for finding out  $\delta^+$  and  $\delta^-$  is given in the Appendix C.

$$\alpha^+ = \frac{P_m^+ - P_{sat}^+}{E_m^+} \quad (2.21)$$

$$\alpha^- = \frac{P_m^- - P_{sat}^-}{E_m^-} \quad (2.22)$$

$$\delta^+ = -\frac{\tan\left[\frac{\pi}{2}\left(\frac{P_m^+ - P_{sat}^+ - 2P_R^-}{P_m^+ + P_{sat}^+}\right)\right]}{E_C^+} \quad (2.23)$$

$$\delta^- = -\frac{\tan\left[\frac{\pi}{2}\left(\frac{P_m^- - P_{sat}^- - 2P_R^+}{P_m^- + P_{sat}^-}\right)\right]}{E_C^-} \quad (2.24)$$

The model is implemented in MATLAB and the simulation result is compared with the experimental hysteresis as shown in the Figure 2.14. The simulation curve still suffers from the saturation issue. It could not reach the maximum polarization value for the maximum applied voltage. All the values of the parameters used for the simulation are same as the experimental values which are listed in the Table 2.4.

Table 2.4: Experimental and MATLAB parameters for J. Yu *et al.* model.

Parameters	Experimental		MATLAB	
	+ve sweep	-ve sweep	+ve sweep	-ve sweep
$E_C$ (V/cm)	$5.145 \times 10^5$	$-4.4549 \times 10^5$	$5.145 \times 10^5$	$-4.4549 \times 10^5$
$P_R$ (C/cm <sup>2</sup> )	$-7.41 \times 10^{-6}$	$7.29 \times 10^{-6}$	$-7.41 \times 10^{-6}$	$7.29 \times 10^{-6}$
$P_S$ (C/cm <sup>2</sup> )	$8.461 \times 10^{-6}$	$-8.2274 \times 10^{-6}$	$8.461 \times 10^{-6}$	$-8.2274 \times 10^{-6}$
$P_{max}$ (C/cm <sup>2</sup> )	$8.461 \times 10^{-6}$	$-8.2274 \times 10^{-6}$	$8.461 \times 10^{-6}$	$-8.2274 \times 10^{-6}$

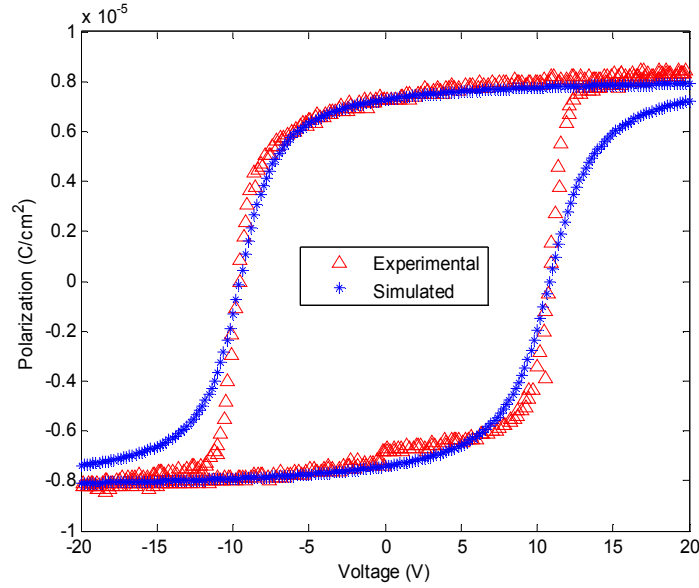


Figure 2.14: Experimental and MATLAB simulated hysteresis curve using J. Yu *et al.* model.

#### 2.4.4 Y. L. Wang *et al.* Model for Polycrystalline Ferroelectrics [20]

A single domain ferroelectric converts into multi-domain ferroelectric during the domain switching process. Hence a single domain model for polarization hysteresis cannot perfectly describe polarization reversal process in the vicinity of coercive field. As an example, the Landau theory for mono-crystalline ferroelectrics given by C. J. Brenann shows an abrupt switching of dipoles at coercive field as explained in Section 2.4.2. A polycrystalline ferroelectric consists of many grains which are formed by lots of unit cells. The polarization distribution of polycrystalline ferroelectrics can be affected by grain orientation, grain size and grain boundary. A polycrystalline ferroelectric may have different grain orientation without applied field but upon the application of applied electric field, it can only have two possible spontaneous polarization states which are upward polarization ( $P_{up}$ ) and downward polarization ( $P_{down}$ ) and they are related as  $P_{up} = -P_{down}$ . The total free energy of the polycrystalline ferroelectrics is the sum of the free energies due to paraelectric state, upward polarization, downward polarization and domain walls.



$$F = F_0 + F_{up} + F_{down} + F_{wall} \quad (2.25)$$

The free energy for a polycrystalline ferroelectric can be expressed in terms of  $P_{up}$  as follows.

$$F = F_0 - \frac{\alpha}{2} P_{up}^2 + \frac{\beta}{4} P_{up}^4 + (1 - 2\alpha_{up}) E P_{up} \quad (2.26)$$

where  $\alpha$  and  $\beta$  are Landau coefficients and  $F_0$  is the free energy in paraelectric state. Here it is considered that  $\alpha_{down} = 1 - \alpha_{up}$ , where  $\alpha_{up}$  and  $\alpha_{down}$  are the volume fractions of upward polarization and downward polarization in the whole volume, respectively. Here  $\alpha_{up}$  includes the free energy part from the domain walls.  $P_{up}$  can be determined when the derivative of above equation is zero.

$$-\alpha P_{up} + \beta P_{up}^3 + (1 - 2\alpha_{up}) E = 0 \quad (2.27)$$

Now the average polarization ( $P$ ) for each values of electric field ( $E$ ) can be determine as,

$$P = \alpha_{up} P_{up} + \alpha_{down} P_{down} = (2\alpha_{up} - 1) P_{up} \quad (2.28)$$

Here,  $P_{up}$  is the spontaneous polarization when the polarization reversal is completely saturated under the applied field. This implies that according to (2.28), the function  $\alpha_{up}$  should depend on applied electric field and reflect the polarization distribution along electric field. The expression for  $\alpha_{up}$  is obtained by fitting the formula with experimental hysteresis which is given as,

$$\alpha_{up} = \frac{\arctan[\beta_1(E - E_c) + \beta_2(E - E_c)^3] + \pi/2}{\pi} \quad (2.29)$$

where  $\beta_1$  and  $\beta_2$  are constants. The value of  $\alpha_{up}$  changes sharply from 0 to 1 in the vicinity of  $E_C$  when the electric field is increased from  $-E_0$  to  $+E_0$ , where  $-E_0$  and  $+E_0$  are minimum and maximum applied electric field respectively. If the applied electric field is not large enough to completely saturate the ferroelectric material at both limits in field, the value of  $\alpha_{up}(E)$  cannot reach 0 or 1 for the applied electric field and the polarization hysteresis losses the symmetry. Replacement of  $\alpha_{up}(E)$  by  $\alpha'_{up}(E)$  has been employed to

restore the symmetry and to improve agreement with experimental results in saturation region.

$$\alpha'_{up}(E) = \alpha_{up}(E) + \frac{1 - \alpha_{up}(E_0) - \alpha_{up}(-E_0)}{2} \quad (2.30)$$

When  $E_0$  is large enough for polarization saturation,  $\alpha_{up}(E_0) = 1$  and  $\alpha_{up}(-E_0) = 0$ , thus  $\alpha'_{up}(E) = \alpha_{up}(E)$ . Hence (2.30) can be applied for both saturated and unsaturated hysteresis loops.

The mathematical model that uses Landau free energy theory for polycrystalline ferroelectrics is implemented in MATLAB to simulate the hysteresis curve and compared with experimental hysteresis as shown in Figure 2.15. Values of the parameters used for the simulation are listed on the Table 2.5. The value of a Landau coefficient  $\alpha$  is calculated using the following formula.

$$\alpha = -(T - T_C) / (\varepsilon_0 \times C) \quad (2.31)$$

Where,  $T_C$  is the ferroelectric Curie-Weiss temperature,  $\varepsilon_0$  is dielectric permittivity of free space and  $C$  is Curie-Weiss constant.

The value of  $P_{up}$  is predicted by solving the cubic equation (2.27) and selecting only the real and the closest to the previous  $P_{up}$  value. The values of  $\alpha$  and  $\beta$  are given in Table 2.5 and  $\alpha_{up}$  is calculated using (2.21).  $P_{up}$  is almost constant and equal to the spontaneous polarization as shown in Figure 2.15. The simulation curve that uses  $\alpha_{up}$  suffers from the polarization saturation problem and asymmetry. This simulation hysteresis is bigger in shape than the experimental hysteresis and also closed loop is not formed as shown in the inset of above Figure. Using  $\alpha'_{up}$  instead of  $\alpha_{up}$  maintains the symmetry even in the unsaturated condition. The hysteresis loop is closed and shows a better agreement with experimental hysteresis as shown in Figure 2.15. This mathematical model shows overall improvement in describing the polarization hysteresis but fails to approximate the slope of the experimental hysteresis in the vicinity of  $E_C$ . This model also has the discontinuity at  $E=0$  which is explained by (2.27) and can be observed in the

Figure 2.15. Another drawback of this approach was that the paradigm presented did not include a systematic analytic scheme to predict the constants  $\beta_1$ ,  $\beta_2$  and  $\beta$ . These constants used in the simulation tests were selected by trial and error to approximately optimize agreement with experimental data.

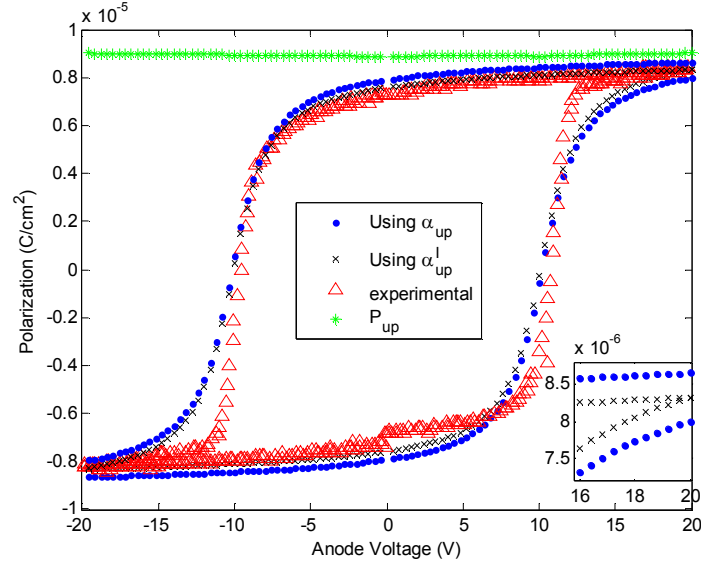


Figure 2.15: Experimental and MATLAB simulated polarization hysteresis using Landau free energy expression by Y. L. Wang *et al.* [20].

Table 2.5: Simulation parameters for the polarization hysteresis of ferroelectric using Landau free energy expression by Y. L. Wang *et al.* [20].

Parameters	Values
$E_C$	$4.847 \times 10^5$ V/cm
$T$	300 K
$\epsilon_0$	$8.8541 \times 10^{-14}$ F/cm
$T_c$	443 K [38]
$C$	500 K [39]
$\beta_1$	$1.2 \times 10^{-5}$ cm/V
$\beta_2$	$-4.357 \times 10^{-19}$ cm <sup>3</sup> /V <sup>3</sup>
$\alpha$	$3.23 \times 10^{12}$ cm/F
$\beta$	$4.1 \times 10^{22}$ cm <sup>5</sup> /F.C <sup>2</sup>

### 2.4.5 Modified Y. L. Wang *et al.* Model

Y. L. Wang *et al.* model gives the formula for calculating  $\alpha$  as in (2.31) but this model does not give the formula for predicting  $\beta$ . In section 2.4.2 it is discussed that  $\alpha$  and  $\beta$  can be calculated if either of them is known as given by (2.7). This is an approach to find  $\alpha$  and  $\beta$  by combining these two models. Knowing the constant  $\alpha$  from (2.31),  $\beta$  can be calculated using (2.7) as follows.

$$\beta = \alpha / P_s^2 \quad (2.32)$$

Table 2.6 includes the calculated value of  $\beta$  which is little higher than previously assumed in Y. L. Wang *et al.* model. To compensate for the increase in  $\beta$  value, the constant  $\beta_1$  is also modified as given in Table 2.6. The corresponding MATLAB simulation is shown in Figure 2.16 which is similar in agreement with experimental as compared with Figure 2.15. With this modification only two constants  $\beta_1$  and  $\beta_2$  are needed to be selected by trial and error.

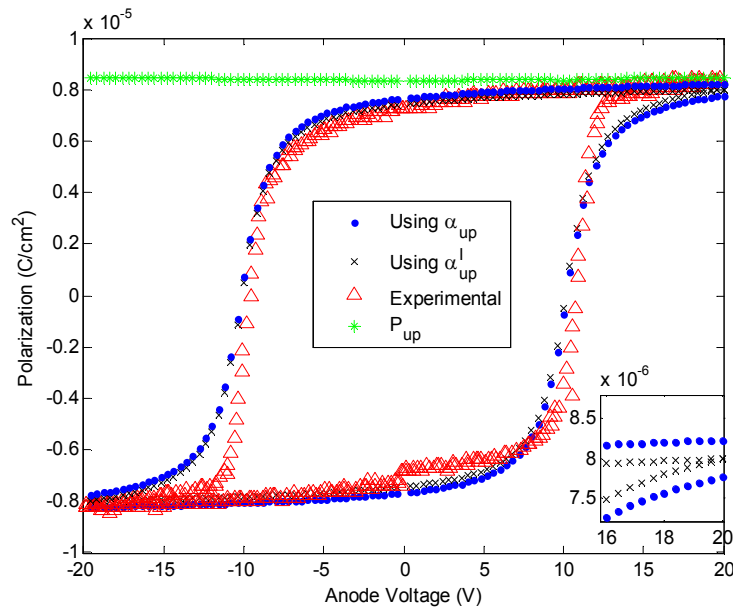


Figure 2.16: Experimental and MATLAB simulated polarization hysteresis using modified Y. L. Wang *et al.* model.

Table 2.6: Simulation parameters for the polarization hysteresis of ferroelectric using modified Y. L. Wang *et al.* model.

Parameters	Values
$P_s$	$8.34 \times 10^{-6} \text{ C/cm}^2$
$\alpha$	$3.23 \times 10^{12} \text{ cm/F}$
$\beta$	$4.6 \times 10^{22} \text{ cm}^5/\text{F.C}^2$
$\beta_1$	$1.6 \times 10^{-5} \text{ cm/V}$
$\beta_2$	$-4.357 \times 10^{-19} \text{ cm}^3/\text{V}^3$

## Chapter 3

### New Models for Predicting Polarization

#### 3.1 Introduction

Although the ferroelectric models discussed in Chapter 2 provided the mathematical and physical formulism to predict polarization hysteresis, they did not give an excellent level of agreement with the experimental data. These models suffered from deficiencies in terms of their ability to correctly replicate saturation and critical slope conditions when compared with experimental data as explained previously. This chapter includes the mathematical models that minimize the shortcomings of above models and give better agreement with experimental hysteresis. In this Chapter, a curve fitting approach is taken to systematically determine the constants needed to describe the coefficient  $\alpha_{up}$  introduced in Y. L. Wang *et al.* model [20]. The initial approach is to predict the parameters for unknown constants  $\beta_1$  and  $\beta_2$  with a two term cubic polynomial as used in the argument of hyperbolic tangent (2.29). To improve the curve fitting other approaches involving two terms cubic with different curve fitting points, standard three terms cubic with three curve fitting points, and four terms standard quadratic with four curve fitting points were also implemented. These approaches were not sufficiently successful in generating a close agreement with experimental curve to warrant inclusion in this thesis work. To improve the slope of the polarization curves in the vicinity of  $E_C$ , other approaches involving the unit step function in the argument of hyperbolic tangent (2.29) are implemented. The approaches involving three matching conditions with a unit step function and four matching conditions with two unit step functions provided a faithful replication of the experimental hysteresis.

### 3.2 Model Based on Predicting Coefficients $\beta_1$ and $\beta_2$

Y. L. Wang *et al.* model does not give the expressions for calculating the coefficients  $\beta_1$ ,  $\beta_2$  and  $\beta$ . Their values are chosen in order to provide a good agreement with experimental hysteresis. The expressions for these constants are derived considering the fact that  $P_{up}$  is the highest polarization value of the experimental hysteresis loop which is spontaneous polarization [20]. This consideration  $P_{up}=P_s$  eliminates the need of calculating  $\alpha$  and selecting  $\beta$  which are ingredients in Y. L. Wang *et al.* model. A curve fitting approach is considered for finding out the values of constants  $\beta_1$  and  $\beta_2$ . Two points on positive going branch hysteresis curve at  $E=0$  and  $E=-E_C$  are considered as shown in Figure 3.1. The expression for the polarization using Y. L. Wang *et al.* model is,

$$P = (2\alpha_{up} - 1)P_{up} \quad (3.1)$$

The polarization at the two points as mentioned above can be written in generalized form as follows. The polarization values at those points are directly extracted from experimental hysteresis and are given in Table 3.1.

$$P_j = (2\alpha_{upj} - 1)P_{up} \quad \text{for } j=1 \text{ and } 2. \quad (3.2)$$

Using (3.2), the normalized polarization is defined as,

$$r_j = \frac{P_j}{P_{up}} = (2\alpha_{upj} - 1) \quad (3.3)$$

For a point in the hysteresis  $\alpha_{up}$  can be calculated if the polarization at that point is known using a formula derived from (3.3).

$$\alpha_{upj} = \frac{(r_j + 1)}{2} \quad (3.4)$$

The formula for the  $\alpha_{up}$  from Y. L. Wang model in generalized form can be written as,

$$X_j = \tan\left(\pi\alpha_{upj} - \frac{\pi}{2}\right) \quad (3.5)$$

where, from the two term cubic used in Y. L. Wang model,

$$X_j = \beta_1(E_j - E_C) + \beta_2(E_j - E_C)^3 \quad (3.6)$$

Data for (3.2)-(3.5) evaluated at the two locations as shown in Figure 3.1 are summarized on Table 3.1.

Table 3.1: Values of the terms for calculating  $\beta_1$  and  $\beta_2$ .

<b>j</b>	<b>E</b>	<b>P<sub>j</sub></b>	<b>r<sub>j</sub></b>	<b><math>\alpha_{upj}</math></b>	<b>X<sub>j</sub></b>
1	0	$-7.35 \times 10^{-6} \text{ C/cm}^2$	-0.881	0.059	-5.3
2	$-E_C$	$-7.994 \times 10^{-6} \text{ C/cm}^2$	-0.958	0.02	-7.66

For the value of  $j=1$  and  $2$ , (3.6) yields two equations.

$$X_1 = \beta_1(-E_C) + \beta_2(-E_C)^3 \quad (3.7)$$

$$X_2 = \beta_1(-2E_C) + \beta_2(-2E_C)^3 \quad (3.8)$$

Equations (3.7) and (3.8) can be solved for the constants  $\beta_1$  and  $\beta_2$  using inverse matrix method as follows.

$$\begin{bmatrix} \beta_1 \\ \beta_2 \end{bmatrix} = M^{-1} \begin{bmatrix} X_1 \\ X_2 \end{bmatrix} = \begin{bmatrix} 9.31 \times 10^{-6} \text{ cm} / V \\ 6.91 \times 10^{-18} \text{ cm}^3 / V^3 \end{bmatrix} \quad (3.9)$$

where, from (3.7) and (3.8) it can be seen,

$$M = \begin{bmatrix} -E_C & -E_C^3 \\ -2E_C & -8E_C^3 \end{bmatrix} \quad (3.10)$$

Now the polarization can be calculated using (3.1) where,

$$\alpha_{up}(E) = \frac{\arctan[X(E)] + \pi/2}{\pi} \quad (3.11)$$

The expression for  $X(E)$  which is consistent with Y. L. Wang *et al.* model is given as,

$$X(E) = \beta_1(E - E_C) + \beta_2(E - E_C)^3 \quad (3.12)$$



The MATLAB simulation of the hysteresis curve by using constants  $\beta_1$  and  $\beta_2$  from (3.8) is compared with experimental hysteresis curve as shown in Figure 3.1. The values of other simulation parameters are same with the average experimental values as given in Table 2.1. Comparison of simulated hysteresis with experimental hysteresis shows an excellent match in the region where the curve matching points are taken but the simulated curve did not exhibit saturation at the maximum applied electric field.

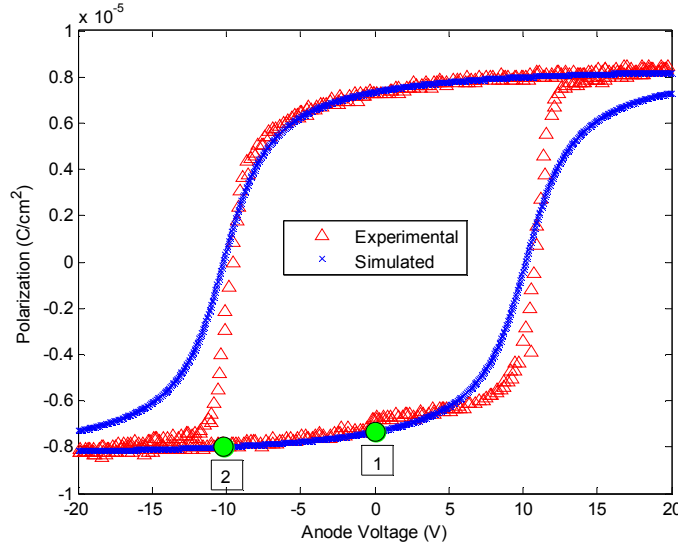


Figure 3.1: Experimental and MATLAB simulated polarization hysteresis of ferroelectric by calculating the constants  $\beta_1$  and  $\beta_2$ .

### 3.3 New Practical Model with Three-point Fit

Above simulation results shows that the expression for  $\alpha_{up}$  is not good enough to fit our experimental hysteresis. In order to force the curve to saturate early and form a closed loop, another point near the saturation level and in the vicinity of  $E_C$  is considered as shown in Figure 3.3. The point is selected at  $E_C(1+z)$  where the value of  $z$  is arbitrarily taken to be 0.2 but should satisfy the following condition.

$$0 < E_C(1 \pm z) < E_{\max} \quad (3.13)$$

Where  $E_{\max}$  is the maximum electric field associated with maximum applied voltage. The expression of  $X_j$  for finding the  $\alpha_{upj}$  is modified as follows.

$$X_j = \beta_1(E_j - E_C) + \beta_2(E_j - E_C)^3 u(E_j - E_C) + \beta_3(E_j - E_C)^5 \quad (3.14)$$

In this expression, a unit step function is considered that forces the polarization to saturate faster on positive side. The unit step function  $u(x)$  is a function whose value is 1 for  $x \geq 1$  and 0 otherwise. Figure 3.2 shows a unit step function which is defined by following equation.

$$u(x) = \begin{cases} 1 & x \geq 1 \\ 0 & \text{otherwise} \end{cases} \quad (3.15)$$

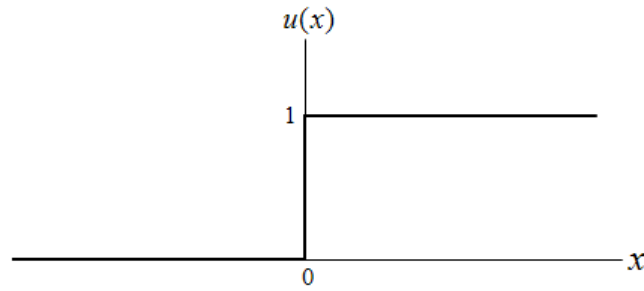


Figure 3.2: Unit step function.

As seen from Figure 3.3, three points are considered on the positive going branch hysteresis and therefore there are three unknown constants  $\beta_1$ ,  $\beta_2$  and  $\beta_3$  to be calculated. Data for (3.2)-(3.5) evaluated at the three points for  $j=1, 2$  and  $3$  as shown in Figure 3.3 are summarized on Table 3.2.

Table 3.2: Values of the terms for calculating  $\beta_1$ ,  $\beta_2$  and  $\beta_3$ .

<b>j</b>	<b>E</b>	<b>P<sub>j</sub></b>	<b>r<sub>j</sub></b>	<b><math>\alpha_{upj}</math></b>	<b>X<sub>j</sub></b>
1	0	$-7.35 \times 10^{-6} \text{ C/cm}^2$	-0.881	0.059	-5.3
2	$-E_C$	$-7.994 \times 10^{-6} \text{ C/cm}^2$	-0.958	0.02	-15.323
3	$E_C(1+z)$	$7.15 \times 10^{-6} \text{ C/cm}^2$	0.857	0.928	4.386

For the values of  $j= 1, 2$  and  $3$ , (3.14) yields three different equations which can be solved for the constants  $\beta_1$ ,  $\beta_2$  and  $\beta_3$  using inverse matrix method as follows.

$$\begin{bmatrix} \beta_1 \\ \beta_2 \\ \beta_3 \end{bmatrix} = M^{-1} \begin{bmatrix} X_1 \\ X_2 \\ X_3 \end{bmatrix} = \begin{bmatrix} 1.061 \times 10^{-5} \text{ cm} / V \\ 3.686 \times 10^{-15} \text{ cm}^3 / V^3 \\ 5.883 \times 10^{-40} \text{ cm}^5 / V^5 \end{bmatrix} \quad (3.16)$$

where

$$M = \begin{bmatrix} -E_C & 0 & (-E_C)^5 \\ -2E_C & 0 & (-2E_C)^5 \\ zE_C & (zE_C)^3 & (zE_C)^5 \end{bmatrix} \quad (3.17)$$

Knowing the values of constants  $\beta_1$ ,  $\beta_2$  and  $\beta_3$  the positive going polarization curve can be plotted using (3.1). The expression for  $\alpha_{up}(E)$  is given by (3.9) and  $X(E)$  can be expressed as,

$$X(E) = \beta_1(E - E_C) + \beta_2(E - E_C)^3 u(E - E_C) + \beta_3(E - E_C)^5 \quad (3.18)$$

The polarization hysteresis curve using three-point fit model is obtained by substituting (3.18) into (3.11) which is finally substituted back into (3.1). The comparison of MATLAB simulation and the experimental polarization hysteresis curve is shown in Figure 3.3.

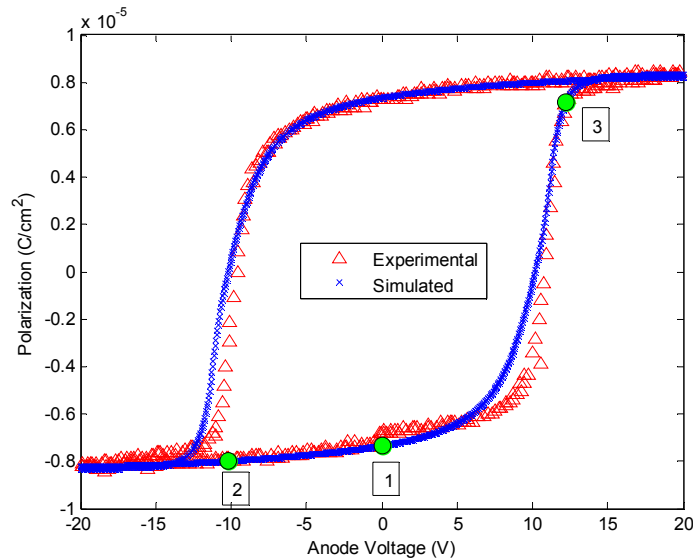


Figure 3.3: Experimental and MATLAB simulated polarization hysteresis of ferroelectric by using new practical model with three-point fit.

The values of other simulation parameters are same with the average experimental values as given in Table 2.1. Comparison of simulated hysteresis with experimental hysteresis shows an improved level of agreement in saturation. The problem of not reaching the polarization saturation point at desired electric field is solved using this model and a complete hysteresis loop is formed. The only region where the simulation curve does not show good level of agreement with experimental hysteresis is the region just below the coercive field. This problem will be taken care in next section.

### 3.4 New Practical Model with Four-point Fit

The need of this model is to give a better level of agreement with the experiment hysteresis in the region below coercive field. It is clear from above section that choosing a point near the saturation level and using unit step function forces the simulation curve to pass through that point. Now we take one more point just below the coercive field as shown Figure 3.4 and use unit step function to increase the slope of simulation curve at that region. The point is selected at  $E_C(1-z)$  where the value of  $z$  is arbitrarily taken to be 0.2 but should generally satisfy the following condition.

$$0 < E_C(1 \pm z) < E_{\max} \quad (3.19)$$

Where  $E_{\max}$  is the maximum electric field associated with maximum applied voltage. The expression for  $X_j$  to find  $\alpha_{upj}$  is modified as follows.

$$X_j = \beta_1(E_j - E_C) + \beta_2(E_j - E_C)^2 u(E_j - E_C) + \beta_3(E_j - E_C)^2 u(E_C - E_j) + \beta_4(E_j - E_C)^3 \quad (3.20)$$

In this expression, two unit step functions are considered that take care of polarization slope changes in the vicinity of the coercive field. Because four points are considered on the positive going branch hysteresis, there are four unknown constants  $\beta_1, \beta_2, \beta_3$  and  $\beta_4$  to be calculated. Data for (3.2)-(3.5) evaluated at the four locations as shown in Figure 3.4 are summarized on the Table 3.3.

Table 3.3: Values of the terms for calculating  $\beta_1$ ,  $\beta_2$ ,  $\beta_3$  and  $\beta_4$ .

j	E	$P_j$	$r_j$	$\alpha_{upj}$	$X_j$
1	0	$-7.41 \times 10^{-6} \text{ C/cm}^2$	-0.875	0.062	-5.06
2	$-E_C$	$-7.994 \times 10^{-6} \text{ C/cm}^2$	-0.944	0.027	-11.5
3	$E_C(1+z)$	$7.68 \times 10^{-6} \text{ C/cm}^2$	0.907	0.953	6.84
4	$E_C(1-z)$	$-5.42 \times 10^{-6} \text{ C/cm}^2$	-0.640	0.179	-1.57

For the values of  $j= 1, 2, 3$  and  $4$ , (3.20) yields three different equations which can be solved for the constants  $\beta_1, \beta_2, \beta_3$  and  $\beta_4$  using inverse matrix method as follows.

$$\begin{bmatrix} \beta_1 \\ \beta_2 \\ \beta_3 \\ \beta_4 \end{bmatrix} = M^{-1} \begin{bmatrix} X_1 \\ X_2 \\ X_3 \\ X_4 \end{bmatrix} = \begin{bmatrix} 1.76 \times 10^{-5} \text{ cm} / V \\ 4.73 \times 10^{-10} \text{ cm}^2 / V^2 \\ 2.40 \times 10^{-11} \text{ cm}^2 / V^2 \\ 1.72 \times 10^{-17} \text{ cm}^3 / V^3 \end{bmatrix} \quad (3.21)$$

where,

$$M = \begin{bmatrix} -E_C & 0 & (-E_C)^2 & (-E_C)^3 \\ -2E_C & 0 & (-2E_C)^2 & (-2E_C)^3 \\ zE_C & (zE_C)^2 & 0 & (zE_C)^3 \\ -zE_C & 0 & (-zE_C)^2 & (-zE_C)^3 \end{bmatrix} \quad (3.22)$$

Knowing the values of constants  $\beta_1, \beta_2, \beta_3$  and  $\beta_4$ , the positive going polarization curve can be plotted by using (3.1). The expression for  $\alpha_{up}(E)$  is given by (3.9) and  $X(E)$  can be expressed as,

$$X(E) = \beta_1(E - E_C) + \beta_2(E - E_C)^2 u(E - E_C) + \beta_3(E - E_C)^2 u(E_C - E) + \beta_4(E - E_C)^3 \quad (3.23)$$

Although the ideal hysteresis curve should be symmetric, our experimental hysteresis is not symmetric. So using the anti-symmetry of  $\alpha_{up}$  to generate the negative going branch polarization curve does not give satisfactory agreement with corresponding experimental negative going branch hysteresis. Similar mathematical approach as used for generating positive going hysteresis can be employed for generating the negative

going hysteresis curve. The four points are taken on the negative going branch curve and  $P_{\text{down}}$  and  $\alpha_{\text{down}}$  are used for mathematical calculation instead of  $P_{\text{up}}$  and  $\alpha_{\text{up}}$ . The detail mathematical expression for generating negative going branch polarization curve using four-point fit model is given in the Appendix D. The values of the parameters used for simulating both parts of the polarization curve are given in Table 3.4. Polarization data  $\{P_1, P_2, P_3, P_4\}$  for negative sweep were taken at the electric fields  $E = \{0, +E_c, -E_c(1+z), -E_c(1-z)\}$  respectively. The MATLAB simulation with this model and experimental hysteresis is compared in Figure 3.4. The simulation curve shows an excellent match with the experimental hysteresis. The problems with most of the ferroelectric hysteresis models of not reaching the saturation level early and polarization curve slope issue are solved using this model as shown in Figure 3.4. The polarization saturation and the slope of the polarization curve depend upon the selection value of the constant 'z'. Lower the value of 'z', faster the polarization saturates and vice versa. So the value of 'z' provides flexibility to our model to be applicable with any other device's experimental hysteresis. Our approach of modeling hysteresis curve is similar to the approach employed by C. Fu *et al.* The positive part of our model is that it considers single polarization domain curves with four unknown constants; whereas C. Fu *et al.* consider three polarization domain curves with nine unknown constants. Our consideration highly reduces the mathematical complexity and also shows the excellent level of agreement with experimental hysteresis curve as shown in Figure 3.4.

Table 3.4: Values of the simulation parameters for polarization hysteresis of ferroelectric by using new practical model with four-point fit.

Parameters	Values (positive sweep)	Values (negative sweep)
$E_c$	$5.145 \times 10^5 \text{ V/cm}$	$-4.549 \times 10^5 \text{ V/cm}$
$P_S$	$8.46 \times 10^{-6} \text{ C/cm}^2$	$-8.22743 \times 10^{-6} \text{ C/cm}^2$
$P_R = P_1$	$-7.41 \times 10^{-6} \text{ C/cm}^2$	$7.2938 \times 10^{-6} \text{ C/cm}^2$
$P_C = P_2$	$-7.994 \times 10^{-6} \text{ C/cm}^2$	$8.0 \times 10^{-6} \text{ C/cm}^2$
$P_3$	$7.68 \times 10^{-6} \text{ C/cm}^2 \text{ (z=0.2)}$	$-7.0 \times 10^{-6} \text{ C/cm}^2 \text{ (z=0.2)}$
$P_4$	$-5.42 \times 10^{-6} \text{ C/cm}^2 \text{ (z=0.2)}$	$5.0 \times 10^{-6} \text{ C/cm}^2 \text{ (z=0.2)}$

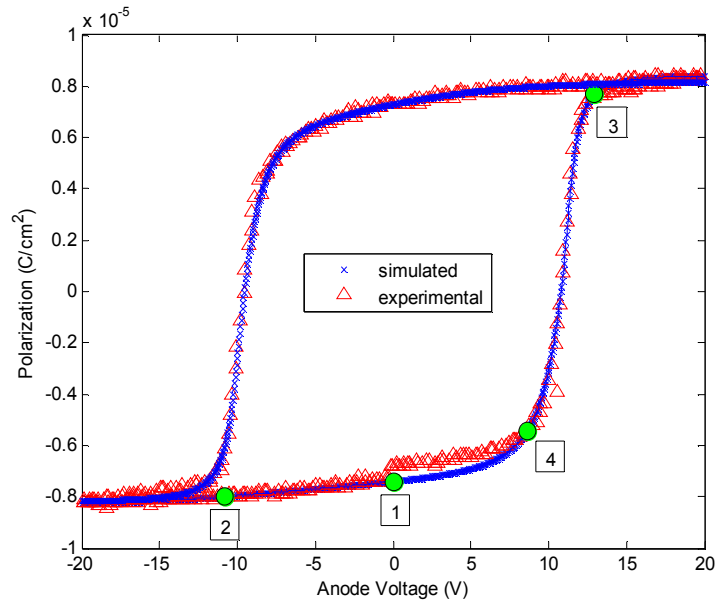


Figure 3.4: Experimental and MATLAB simulated polarization hysteresis of ferroelectric by using new practical model with four-point fit.

## **Chapter 4**

### **Capacitance Modeling**

#### **4.1 Introduction**

Capacitance (C)-Voltage (V) hysteresis characteristic is one of the most well known behaviors of the ferroelectric capacitors [40]. Since ferroelectric capacitance is directly proportional to ferroelectric permittivity and the ferroelectric permittivity is field dependent, the ferroelectric capacitance also depends on the applied field. The C-V hysteresis of a ferroelectric capacitor is caused by the polarization orientation under the applied field [40]. Ferroelectric permittivity is very large about the coercive field because a very small change in electric field near the coercive field causes a very large change in the ferroelectric polarization. Ferroelectric permittivity is the highest when ferroelectric capacitor is neutral or not polarized [41] that explains the formation of peaks at positive and negative coercive field on a C-V hysteresis. The C-V characteristic of a ferroelectric capacitor is also affected by the space-charge concentration at the ferroelectric to contact interface because it has an adverse effect on permittivity and switching characteristics [41]. Spontaneous polarization produces a high electric field that causes band bending and ionization of trap states. This phenomenon causes the formation of space charge at the contacts to screen the polarization of the ferroelectric which lowers the permittivity. Therefore a ferroelectric capacitor can be viewed as having three layers with high permittivity layer sandwiched between two low permittivity layers [41].

There are two ways of obtaining the capacitance of a ferroelectric capacitor [42, 22]. One way is by measuring the capacitance directly with small ac signal together with slow varying dc bias. The capacitance curve measured by this method is called the small-signal capacitance. The experimental capacitance curve shown in Fig 2.9 is small signal capacitance. Another method of obtaining capacitance is by taking the derivative of its



polarization hysteresis loop which is called large-signal capacitance. Analyses have shown that the peak values of large-signal C-V curves are sharper and higher than that of small-signal C-V curves [42, 22]. Ferroelectric thin films are used with large signal in the memory applications whereas they are used with small signal in the application as tuning varactor. This implies that for the proper application of ferroelectric thin films, its large signal and small signal performance should be investigated in detail [22]. In this chapter, large signal capacitance is obtained using modified S. L. Miller *et al.* model and our new four-point fit model. Finally a small signal capacitance model by H. Li is implemented in MATLAB and compared with our C-V hysteresis.

## 4.2 Large-Signal Capacitance Modeling

A general expression for finding the large signal capacitance of a ferroelectric capacitor is derived considering the theory from the physics. When an electric field is applied in a dielectric material, the bound charges in the material are separated inducing electric dipole moment. This electric displacement field (D) is defined by [43],

$$D = \varepsilon_0 E + P_{tot} \quad (4.1)$$

where E is the applied electric field,  $\varepsilon_0$  is the vacuum permittivity and  $P_{tot}$  is the total polarization which is the sum of the polarization due to linear displacement and polarization due to ferroelectric switching dipoles.

$$P_{tot} = P_l + P_f \quad (4.2)$$

Polarization due to linear displacement is defined as,

$$P_l = \varepsilon_0 \chi_l E \quad (4.3)$$

where  $\chi_l$  is the electric susceptibility of the ferroelectric which is related to the relative permittivity of the ferroelectric as,

$$\varepsilon_r = 1 + \chi_l \quad (4.4)$$

Using (4.2), (4.3) and (4.4), the expression for D can be written as,

$$D = \varepsilon_0 E + \varepsilon_0 \chi_l E + P_f = \varepsilon_0 \varepsilon_r E + P_f \quad (4.5)$$

In a capacitor, the electric displacement field is equal to the surface charge density ( $\sigma$ ) which is defined as charge per unit surface area.

$$D = \sigma = Q/A \quad (4.6)$$

From (4.5) and (4.6),

$$Q = A(\epsilon_0 \epsilon_r E + P_f) \quad (4.7)$$

The capacitance of a ferroelectric capacitor is defined as,

$$C = \frac{dQ}{dV} = \frac{1}{t} \frac{dQ}{dE} = \frac{A}{t} \left( \epsilon_0 \epsilon_r + \frac{dP_f}{dE} \right) \quad (4.8)$$

where  $t$  is the thickness of ferroelectric dielectric. The expression for  $dP_f / dE$  depends on the model used to find  $P_f$ . Two models for finding  $P_f$  are considered and applied to obtain large signal capacitance as given in following sections.

#### 4.2.1 Large-Signal Capacitance Modeling Using S. L. Miller *et al.* Model

The expression of polarization hysteresis from Miller *et al.* model can be modified to develop the equations which define the relationship between applied voltage and capacitance of the ferroelectric capacitor. Because polarization hysteresis is used to obtain the ferroelectric capacitance in this model, the capacitance obtained is large signal capacitance. The derivative of the polarization given in (2.2) defined by S. L. Miller *et al.* model yields,

$$\frac{dP_d^+(E)}{dE} = P_s \left[ \frac{1}{2\delta} \sec h^2 \left( \frac{E - E_c}{2\delta} \right) \right] \quad (4.9)$$

which is based on math identity given as [37],

$$\frac{d}{dx} \tanh u = \sec h^2 u \frac{du}{dx} \quad (4.10)$$

Using (4.9) in (4.8), the expression for large signal capacitance is,

$$C = \frac{A}{t} \epsilon(E) \quad (4.11)$$

$\epsilon(E)$  is the field dependent permittivity for the ferroelectric capacitors given by [36],

$$\varepsilon(E) = \varepsilon_0 \varepsilon_r + \left[ \frac{P_s}{2\delta} \operatorname{sech}^2 \left( \frac{E - E_C}{2\delta} \right) \right] \quad (4.12)$$

This mathematical expression is implemented within Silvaco's ATLAS device simulator for ferroelectrics and MATLAB. The simulation results are shown in the Figure 4.1 and Figure 4.2. The values of the parameters for both the simulations are exactly same with the experimental values as given in Table 2.1. The value of relative permittivity used for P(VDF-TrFE) is 10 [44].

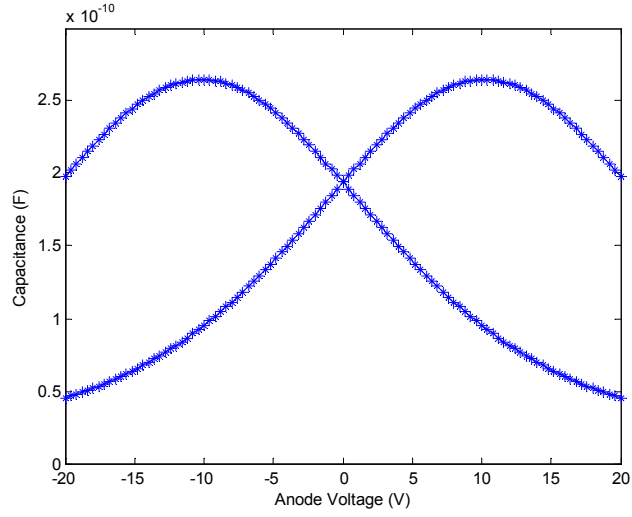


Figure 4.1: MATLAB simulated large signal C-V curve using modified Miller *et al.* model.

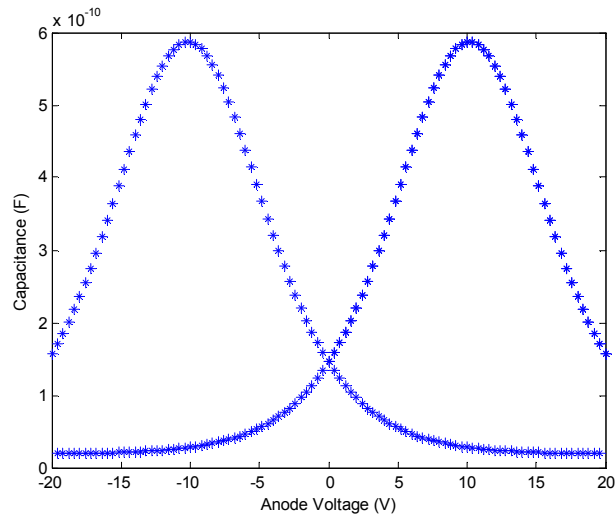


Figure 4.2: Silvaco simulated large signal C-V curve using modified Miller *et al.* model.

As expressed by (4.11), the permittivity of the ferroelectric material changes with respect to electric field and capacitance changes accordingly. When  $E=E_C$ , the field dependent permittivity is maximum according to (4.11) and it is visible on both the simulation curves. Though both of the simulation curves are generated using the same mathematical model, they are not identical. Due to limitations in the availability of Silvaco source code a thorough comparison of Miller model implementation by Silvaco is not possible. The capacitance curves simulated using this model is large-signal capacitance but the experimental capacitance curve is small-signal capacitance, hence no graphical comparison is made between them. As demonstrated The peaks of both large-signal simulation curves are higher but not sharper than the experimental small-signal C-V curve.

#### 4.2.2 Large-Signal Capacitance Modeling Using New Four-point Fit Model

The proposed four-point curve fitting algorithm for the polarization data which was discussed in section 3.4 is used to find the large signal capacitance. This model considers the following expression of polarization.

$$P = (2\alpha_{up} - 1)P_{up} \quad (4.13)$$

where

$$\alpha_{up} = \frac{\arctan(x) + \pi/2}{\pi} \quad (4.14)$$

$$x = \beta_1(E - E_c) + \beta_2(E - E_c)^2 u(E - E_c) + \beta_3(E - E_c)^2 u(E_c - E) + \beta_4(E - E_c)^3 \quad (4.15)$$

Taking the derivative of (4.13) with respect to E and using (4.14) and (4.15),

$$\frac{dP}{dE} = 2P_{up} \frac{1}{\pi} \frac{1}{(1+x^2)} \frac{dx}{dE} \quad (4.16)$$

which makes use of the math identity [37],

$$\frac{d}{dx} \tan^{-1} y = \frac{1}{1+y^2} \frac{dy}{dx} \quad (4.17)$$

Taking the derivative of (4.15) with respect to  $E$ ,

$$\frac{dx}{dE} = \beta_1 + 2\beta_2(E - E_C)u(E - E_C) + 2\beta_3(E - E_C)u(E_C - E) + 3\beta_4(E - E_C)^2 \quad (4.18)$$

For clarity it should be noted that the impulse functions singularities generated by differentiating unit step functions at  $E = \pm E_C$  in expression (4.15) do not appear in (4.18) due to zero factor multipliers at  $E = \pm E_C$ . The differentiation of unit step function is given by [37],

$$\frac{d}{dy}u(y) = \delta(y) \quad (4.19)$$

Using (4.16) and (4.17) in (4.8), the large-signal capacitance can be obtained. This mathematical model is implemented in MATLAB and the simulation result is compared with experimental small-signal capacitance as shown in the Figure 4.3. The experimental small-signal capacitance curve is scaled by 200 times to make a visible overlay with the analytic large-signal capacitance. The values of the parameters used for this simulation are same as tabulated in Table 3.4.

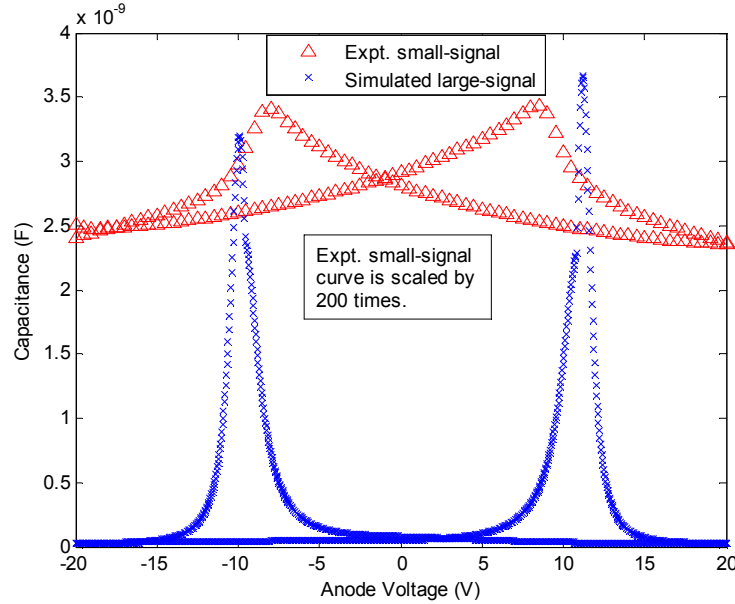


Figure 4.3: Overlay of analytic large-signal and experimental small-signal capacitance.

The analytic large-signal capacitance simulation curve has very sharp peaks and the peak values are much higher than that for experimental small signal capacitance which can be observed from Figure 4.3. This model satisfies the analysis stated in H. Li *et al.* that large-signal capacitance has higher and sharper peaks than small-signal capacitance curve. The asymmetry of our experimental polarization hysteresis causes the two peaks of the large-signal capacitance curve not to be at the same capacitance value.

As described by (4.8), ferroelectric capacitance depends on the derivative of its polarization hysteresis. Since experimental data for the polarization hysteresis is provided [33], an approach that uses the numerical derivative from the experimental polarization hysteresis is also implemented. The expression for large-signal capacitance using numerical derivative approach is given by,

$$C_{num} = A \left( \frac{\epsilon_0 \epsilon_r}{t} + \frac{\Delta P_{exp}}{\Delta V} \right) \quad (4.20)$$

The large-signal capacitance curve generated using point to point numerical derivative method is shown in Figure 4.4. It can be seen that considering all the data points for numerical derivative, the calculate large-signal capacitance is highly noisy.

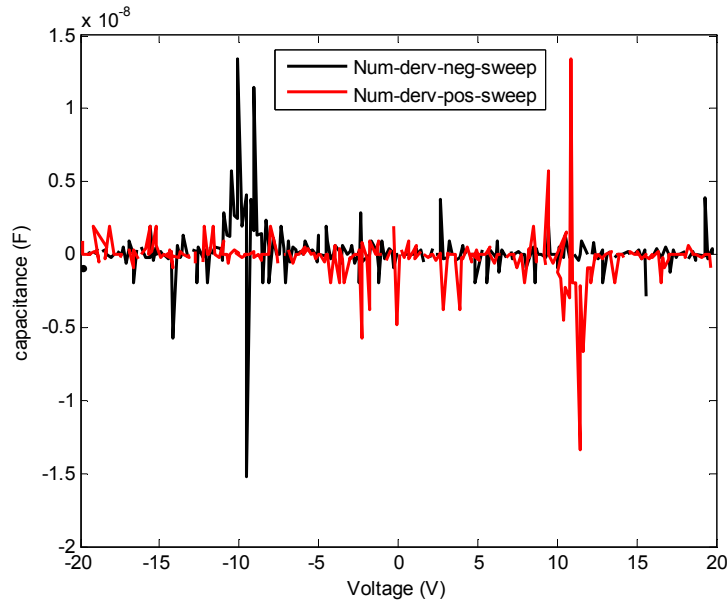


Figure 4.4: Large-signal capacitance using point to point numerical derivative.

In order to produce less noisy large-signal capacitance curve, the derivative is taken by skipping every three points and the result is compared with analytical approach of finding large-signal capacitance as shown in Figure 4.5. Though this approach discards the mathematical complexity issue of curve fitting algorithm, the simulated capacitance curve using this approach is still fairly noisy as compared to the analytical four-point fit approach as shown in Figure 4.5.

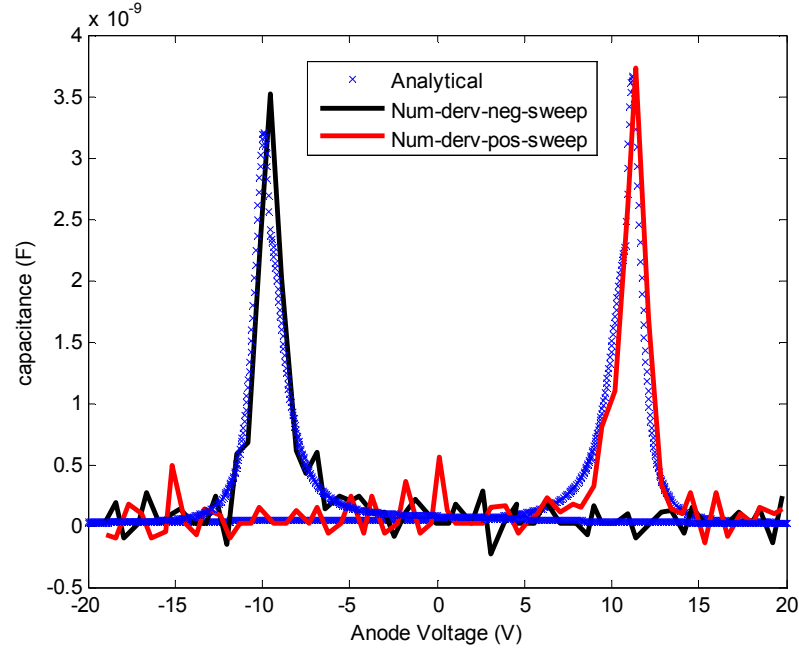


Figure 4.5: Overlay of large-signal capacitance produced using analytical approach and numerical derivative approach by skipping every three points.

### 4.3 Small-Signal Capacitance Modeling

Usually ferroelectric capacitance measurements are performed with a small applied ac voltage whereas analyses of the capacitance are performed by the derivative of the polarization hysteresis [22]. The difference between large-signal and small-signal capacitance is because of the change in space charge in the film during small-signal capacitance measurement [42, 22]. D. Bolten *et al.* gave that the small-signal capacitance is attributed to reversible polarization and domain wall motion but the detail mechanism and its relationship with large-signal capacitance were not addressed [22, 45]. In this

section, a theoretical mechanism of small-signal capacitance is explained using Landau-Khalatnikov kinetic equation which is given by [22, 46],

$$\gamma \frac{dP}{dt} = -\frac{dF}{dP} \quad (4.17)$$

where  $\gamma$  is polarization damping constant or kinetic coefficient [47] and  $F$  is the Landau free energy. Ferroelectric capacitance is proportional to its permittivity, which is directly related to ferroelectric polarization. The total polarization of a ferroelectric capacitor is contributed by switching dipoles as well as the linear polarization. So a ferroelectric capacitor can be modeled into the circuit as shown in the following figure.

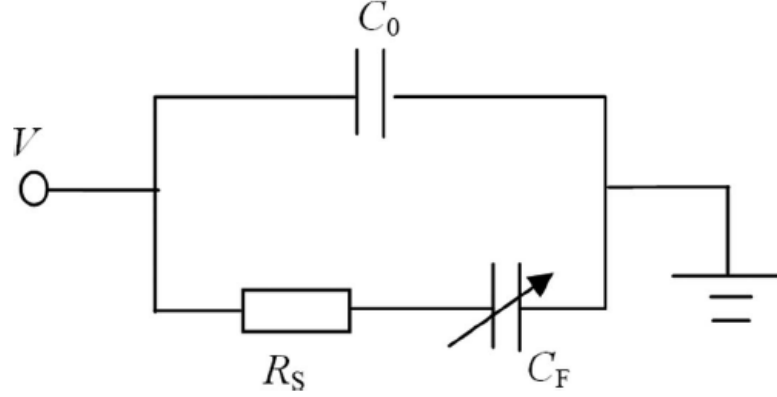


Figure 4.6: Circuit model of a ferroelectric capacitor [22, 48].

In the above figure,  $C_0$  is the linear capacitance,  $C_F$  is the capacitance due to dipole polarization and  $R_S$  is the dipole resistance determined by material properties and dimensions as given below.

$$R_S = \gamma L / A \quad (4.18)$$

Where,  $L$  is the thickness of the ferroelectric film and  $A$  is the cross-sectional area. Assuming  $C_0$  to be very small, the Landau-Khalatnikov dynamic equation for the above circuit can be written as [22, 48],

$$-L \left[ \alpha \left( \frac{Q}{A} \right) + \beta \left( \frac{Q}{A} \right)^3 \right] + V = R_S \frac{dQ}{dt} \quad (4.19)$$



where  $\alpha$  and  $\beta$  are Landau coefficients which are calculated using (2.7) and (2.8),  $Q$  is the charge in the ferroelectric given by (4.7). Taking the derivative of (4.19) with respect to  $V$  and after arranging the terms leads to,

$$C = \frac{dQ}{dV} = \frac{A \left( 1 - R_s \frac{d^2 Q}{dV dt} \right)}{L \left( \alpha + 3\beta Q^2 / A^2 \right)} \quad (4.20)$$

Applying  $\frac{d}{dt} = \omega$ , where  $\omega = 2\pi f$  and solving for  $\frac{dQ}{dV}$  from (4.20), the expression for the small-signal capacitance becomes,

$$C = \frac{dQ}{dV} = \frac{C_{ideal}}{1 + C_{ideal} R_s 2\pi f} \quad (4.21)$$

where, the ideal capacitance is taken as the large-signal capacitance given as [22],

$$C_{ideal} = \frac{A}{L \left( \alpha + 3\beta Q^2 / A^2 \right)} \quad (4.22)$$

The detail derivation for small-signal capacitance is given in Appendix E. According to (4.21), the small-signal capacitance is dependent on the frequency ( $f$ ) of the ac signal. The value of small-signal capacitance decreases with increase in the frequency of ac signal. As capacitance is dependent on charge and charge is related to polarization as given in (4.7), our new model with four-point fit is applied to calculate the polarization. The MATLAB simulation of this small-signal capacitance model and the experimental capacitance curve are compared in Figure 4.7 and the values of the simulation parameters are given in Table 4.1. The comparison of simulation curve for small signal capacitance with experimental capacitance demonstrates much better level of agreement as shown in Figure 4.7 than seen with large signal capacitance. Although the shape of the simulation capacitance hysteresis does not match perfectly with experimental hysteresis, the peak values of the simulation curve show excellent level of agreement with experimental peaks.

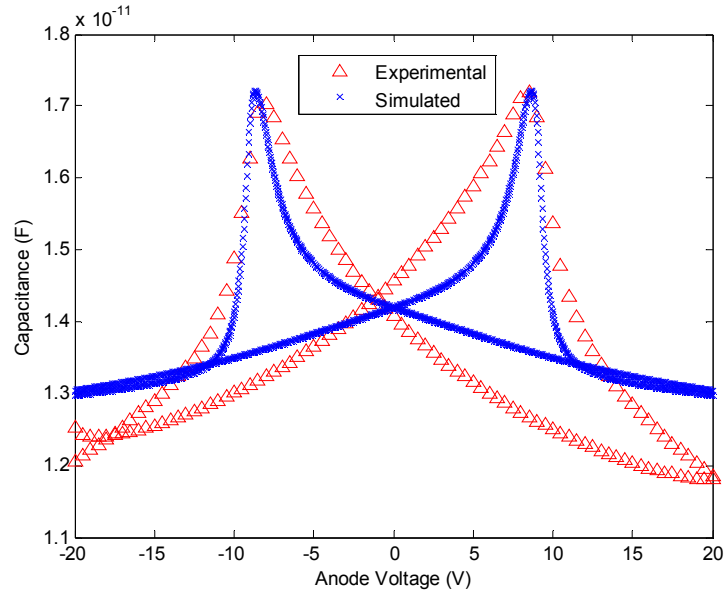


Figure 4.7: Experimental and MATLAB simulated small-signal capacitance curve.

Table 4.1: Values of MATLAB simulation parameters for small-signal capacitance modeling.

Parameters	Values
Kinetic coefficient ( $\gamma$ )	$2 \times 10^5 \Omega\text{-cm}$
ac frequency (f)	$1 \times 10^6 \text{ Hz}$
Device area (A)	$0.0005 \text{ cm}^2$
Film thickness (L)	$210 \times 10^{-7} \text{ cm}$
$R_s$	$8400 \Omega$
$\epsilon_0$	$8.8541 \times 10^{-14} \text{ F/cm}$
$\epsilon_r$	10
$\alpha$	$1.27 \times 10^{11} \text{ cm/F}$
$\beta$	$1.77 \times 10^{21} \text{ cm}^5/\text{F.C}^2$

## Chapter 5

### Conclusion and Future Work

#### 5.1 Conclusion

A brief overview of ferroelectric capacitor, its basic properties and its potential in memory applications were discussed. Characterization techniques of the polarization hysteresis for a ferroelectric capacitor based on polymer P(VDF-TrFE) have been studied. Models, based on physical electronic descriptions [16, 17, 20] were implemented and results were compared with the experimental curve which showed limited agreement. An approach of predicting Landau coefficient  $\beta$  from  $\alpha$  using Landau theory for monocrystalline ferroelectrics, where  $\alpha$  comes from Y. L. Wang *et al.* model was also implemented in the MATLAB. Although this model provided a valuable extension of the Y. L. Wang *et al.* model, the result showed a limited agreement with experimental hysteresis. The problem with these models is that they were unable to reach the polarization saturation fast enough with desired electric field to produce satisfactory overlap with the experimental data. A mathematical derivation for calculating the values of the constants  $\beta_1$  and  $\beta_2$  from the Y. L. Wang *et al.* model, using curve fitting, was presented. Although improved on prior results, the two-point curve fitting was still not in satisfactory agreement with experimental data for all points along the polarization curve. Finally a model free of the polarization saturation issue was derived using an expanded four-point curve fitting algorithm. This model was implemented in MATLAB which showed an excellent level of agreement with experimental hysteresis. This curve fitting approach requires only four unknown constants which is significantly simpler than a previous approach [18] for modeling polarization curves requiring nine unknown constants.

The two ways of obtaining the capacitance of a ferroelectric capacitor were discussed. The large- signal capacitance was obtained by the derivative of the polarization hysteresis generated using S. L. Miller *et al.* model and our new four-point fit model. The mathematical expressions were implemented in the MATLAB simulation tool. Landau-Khalatnikov kinetic equation was used to derive the mathematical expression for small-signal capacitance and the simulation result was compared with experimental capacitance curve which showed a good level of agreement. The simulations of large and small signal capacitance also proved the fact that the peak values of large-signal C-V curves are sharper and higher than that of small-signal C-V curves.

## 5.2 Future work

The new four-point fit model works fine for our experimental data based on AU-P(VDF-TrFE)-AU ferroelectric capacitor. This new model needs to be tested for other set of experimental data based on different ferroelectric materials in order to confirm the applicability of the model.

The large-signal capacitances predicted from S. L. Miller *et al.* model using Silvaco and MATLAB simulations are expected to be consistent. The cause of discrepancy between them needs to be reviewed. Limits in performing the review are expected as the source code for Silvaco software is not made available. Although the peaks of the small-signal capacitance curve shows good level of agreement with experimental peaks, the overall shape of the curve does not give a good match with experimental capacitance. This implies that further detail inspection on mathematical formulation of the small-signal capacitance is needed.

In this work, only simulations of the ferroelectric capacitors are considered. Transistors using ferroelectric materials as gate oxides are also excellent memory devices. For the memory applications, ferroelectric capacitors should be connected along with transistors in the circuit. So the simulations of transistors with ferroelectric gate oxide and the simulation of ferroelectric capacitors in the circuit are recommended to further analyze the ferroelectric materials for use in memory applications.

### **5.3 Sponsor Acknowledgement**

We gratefully acknowledge the US Department of Defense (DOD) for support of this work (Army Research Office Contract W911NF-07-2-0059). We also wish to thank the fabrication group at University of Texas at Dallas for providing stimulating discussions which motivated this study.

## References

- [1] C. H. Ahn, K. M. Rabe and J. M. Triscone, "Ferroelectricity at the Nanoscale: Local Polarization in Oxide Thin Films and Heterostructures", *Science*, Vol. 303, pp. 488-491, 23 Jan 2004.
- [2] Youn Jung Park, Hee June Jeong, Jiyoun Chang, Seok Ju Kang, and Cheolmin Park, "Recent Development in Polymer Ferroelectric Field Effect Transistor Memory", *Journal of Semiconductor Technology and Science*, Vol. 8, No. 1, pp. 51-65, March 2008.
- [3] Soon- Won Jung, Jong-Keun Lee, Young Soon Kim, Sung-Min Yoon, In-Kyu You, Byoung-Gon Yu and Yong-Young Noh, "Top-gate Ferroelectric Thin-Film-Transistors with P(VDF-TrFE) Copolymer", *Current Applied Physics*, 2010, doi:10.1016/j.cap.2009.12.014.
- [4] N. Setter, Damjanovic, L. Eng, G. Fox, S. Gevorgian, S. Hong, A. Kingon, H. Kohlstedt, N. Y. Park, G. B. Stephenson, I. Stolitchnov, A. K. Taganstev, D. V. Taylor, T. Yamada and S. Streiffer, "Ferroelectric Thin Films: Review of Materials, Properties, and Applications", *Journal of Applied Physics*, Vol. 100, 051606 (46 pp.), 2006.
- [5] L. E. Cross and R. E. Newnham, "History of Ferroelectrics", *Ceramics and Civilization*, Vol. 1, Huh-Technology Ceramics-Past, Present, and Future, Copyright by The American Ceramic Society. Inc., 1987.
- [6] M. E. Lines and A. M. Glass, *Principles and Applications of Ferroelectrics and Related Materials*, Oxford University Press, Oxford, reprinted 2009.
- [7] Sergei V Kalinin, Anna N Morozovska, Long Qing Chen and Brian J Rodriguez, "Local Polarization Dynamics in Ferroelectric Materials", *Reports on Progress in Physics*, Vol. 73, 056502 (67 pp.), 2010.
- [8] A. F. Devonshire, "Some Recent Work on Ferroelectrics", *Reports on Progress in Physics*, Vol. 27, No. 1, 1964.

- [9] K. M. Rabe, M. Dawber, C. Lichtensteiger, C. H. Ahn and J. M. Triscone, “Modern Physics of Ferroelectrics: Essential Background”, K. Rabe, Ch. H Ahn and J. M. Triscone, *Physics of Ferroelectrics, A Modern Perspective*, Springer, Verlag Berlin Heidelberg, pp. 1-30, 2007.
- [10] J. T. Wang, C. Zhang and Y. S. Fu, “ Ferroelectric/ Piezoelectric Materials and Their Applications in Advanced Sciences and Technologies”, *International Journal of Modern Physics B*, Vol. 19, Nos. 1, 2 &3, pp. 553-557, 2005.
- [11] Ronald C. G. Naber, Kamal Asadi, Paul W. M. Blom, Dago M. de Leeuw and Bert de Boer, “Organic Nonvolatile Memory Devices Based on Ferroelectricity”, *Advanced Materials*, Vol. 21, pp. 1–13, 2009.
- [12] Kenji Uchino, *Ferroelectric Devices*, Marcel Dekker Inc., 270 Madison Avenue, NY, 10016, 2000.
- [13] Dragan Damjanovic, “Hysteresis in Piezoelectric and Ferroelectric Materials”, I. Mayergoyz and G.Bertotti, *The Science of Hysteresis*, Elsevier, Vol. 3, pp. 337-465, 2005.
- [14] Kiyoshi Nishimura, “Ferroelectric Hysteresis Loop Model of Imprint Properties”, *Electronics and Communications in Japan*, Part 2, Vol. 82, No. 10, pp. 857-864, 1999.
- [15] Peng Gang, Yu Jun, Wang Yunbo, Wang Longhai and Li Jia, “A Model for the Hysteresis Loop’s Simulation of Ferroelectric Capacitors”, *Integrated Ferroelectrics*, Vol. 89, pp. 45–54, 2007.
- [16] S. L. Miller, R. D. Nasby, J. R. Schwank, M. S. Rodgers and P. V. Dressendorfer, “Device Modeling of Ferroelectric Capacitors”, *Journal of Applied Physics*, Vol. 68, No. 12, pp. 6463-6471, 15 Dec 1990.
- [17] Jun Yu, Longhai Wang, Yunbo Wang, Gang Peng, Feng Liu and Junxiong Gao, “A Compact Model for the Simulation of Ferroelectric Capacitor”, *Integrated Ferroelectrics*, Vol. 75, pp. 35–45, 2005.
- [18] Chunlin Fu, Chuanren Yang, Hongwei Chen and Liye Hu, “Model for Dielectric Nonlinearity of Ferroelectrics”, *Journal of Applied Physics*, Vol. 97, 034110 (4 pp.), 2005.
- [19] Ciaran J. Brennan, “A Physical Model for the Electrical Hysteresis of Thin-Film Ferroelectric Capacitors”, *Ferroelectrics*, Vol. 132, pp. 245-257, 1992.

- [20] Ying-Long Wang, Xing-Yuan Wang, Li-Zhi Chu, Ze-Chao Deng, Wei-Hua Liang, Bao-Ting Liu, Guang-Sheng Fu, N. Wongdamnern, T. Sareein and R. Yimnirun, "Simulation of Hysteresis Loops for Polycrystalline Ferroelectrics by an Extensive Landau-Type Model", *Physics Letters A*, Vol. 373, pp. 4282-4286, 2009.
- [21] Bikash Shrestha, Ron Pieper, Wudyalew Wondmagegn, Duo Mao, Israel Mejia, Harvey Stiegler, Bruce E Gnade, Manuel Quevedo-Lopez, "A Practical Model to Analytically Characterize the Polarization Hysteresis of Ferroelectric Capacitors", in Proceedings of the 44<sup>th</sup> IEEE Southeastern Symposium on System Theory, Jacksonville, FL, pp. 40-44, March 2012.
- [22] Huadong Li and Guru Subramanyam, "Capacitance of Thin-Film Ferroelectrics Under Different Drive Signals", *IEEE Transactions on Ultrasonics, Ferroelectrics, and Frequency Control*, Vol. 56, No. 9, pp. 1861-1867, September 2009.
- [23] Rafael Plonka, *Impact of the Interface on the Paraelectric-to-Ferroelectric Phase Transition in Epitaxial BaSrTiO<sub>3</sub> Thin Film Capacitors*, Berichte des Forschungszentrums Jülich, 2007.
- [24] Ronald E. Cohen, "Origin of Ferroelectricity in Perovskite Oxides", *Nature*, Vol. 358, pp. 136-138, 9 July 1992.
- [25] J. C. Burfoot and G. W. Tyler, *Polar Dielectrics and Their Applications*, University of California press, Berkeley and Los Angeles, 1979.
- [26] Ralph C. Smith and Craig L. Hom, "A Domain Wall Theory for Ferroelectric Hysteresis", *Journal of Intelligent Material Systems and Structure*, Vol. 10, Issue 3, pp. 195-213, 1999.
- [27] Z.-Y. Cheng, V. Bharti, T.-B. Xu, Haisheng Xu, T. Mai and Q.M. Zhang, "Electrostrictive Poly(vinylidene Fluoride-trifluoroethylene) Copolymers", *Sensors and Actuators A*, Vol. 90, pp. 138-147, 2001.
- [28] Ryousuke Tamura, Eunju Lim, Shuhei Yoshita, Takaaki Manaka and Mitsumasa Iwamoto, "Analysis of Threshold Voltage Shift of Pentacene Field Effect Transistor with Ferroelectric Gate Insulator as a Maxwell–Wagner Effect", *Thin Solid Films*, Vol. 516, pp. 2753–2757, 2008.
- [29] Seok Ju Kang, Insung Bae, Youn Jung Park, Tae Ho Park, Jinwoo Sung, Sung Cheol Yoon, Kyung Hwan Kim, Dong Hoon Choi, and Cheolmin Park, "Non-volatile Ferroelectric Poly(vinylidene fluoride-co-trifluoroethylene) Memory Based on a Single-Crystalline Tri-isopropylsilylethynyl Pentacene Field-Effect Transistor", *Advanced Functional Materials*, Vol. 19, pp. 1609–1616, 2009.



- [30] Wonjun Choi, Seok Hwan Noh, D. K. Hwang, Jeong-M. Choi, Sungjin Jang, Eugene Kim and Seongil Im, "Pentacene-Based Low-Leakage Memory Transistor with Dielectric/Electrolytic/Dielectric Polymer Layers", *Electrochemical and Solid-State Letters*, Vol. 11, No. 3, pp. H47-H50, 2008.
- [31] V. S. Bystrov, N K Bystrova, E V Paramonova, G Vizdrik, A V Saprionova, M Kuehn, H Kliem and A L Kholkin, "First Principle Calculations of Molecular Polarization Switching in P(VDF-TrFE) Ferroelectric Thin Langmuir-Blodgett Films", *Journal of Physics: Condensed Matter*, Vol. 19, 456210 (15 pp.), 2007.
- [32] Zhijun Hu, Mingwen Tian, Bernard Nysten and Alain M. Jonas, "Regular Arrays of Highly Ordered Ferroelectric Polymer Nanostructures for Non-Volatile Low-Voltage Memories", *Nature Materials*, Vol. 8, pp. 62-67, Jan 2009.
- [33] D. Mao, M.A. Quevedo-Lopez, H. Stiegler, B. E. Gnade and H. N. Alshareef, "Optimization of Poly(vinylidene fluoride-fluoroethylene) Films as a Non-Volatile Memory for the Flexible Electronics.", *Organic Electronics*, Vol. 11, pp. 925-932, 2010.
- [34] D. Mao, I. Mejia, H. Stiegler, B. E. Gnade and M. A. Quevedo-Lopez, "Polarization Behavior of Poly(vinylidene fluoride-fluoroethylene) Copolymer Ferroelectric Thin Film Capacitors for Nonvolatile Memory Application in Flexible Electronics", *Journal of Applied Physics*, Vol. 108, 094102 (6 pp.), 2010.
- [35] Longhai Wang, Jun Yu, Yunbo Wang, Gang Peng, Feng Liu, and Junxiong Gao, "Modeling Ferroelectric Capacitors Based on the Dipole Switching Theory", *Journal of Applied Physics*, Vol. 101, 104505 (7 pp.), 2007.
- [36] Silvaco Data Systems, 4701 Patric Henry Drive, Bldg. 6, Santa Clara, CA 95054, Ph: 408-567-1000.
- [37] Murray R. Spiegel and John Liu, *Mathematical Handbook of Formulas and Tables*, 2<sup>nd</sup> Edition, Schaum's outline series McGraw-Hill, New York, 1999.
- [38] G. Teyssedre, A. Bernes and C. Lacabanne, "Cooperative Movements Associated with the Curie Transition in P(VDF-TrFE) Copolymers", *Journal of Polymer Science Part B: Polymer Physics*, ISSN: 08876266, Vol. 33, Issue 6, 30 April 1995.
- [39] Eiichi Fukada, "History and Recent Progress in Piezoelectric Polymers", *IEEE Transactions on Ultrasonics, Ferroelectrics and Frequency Control*, Vol. 47, No. 6, pp. 1277-1290, Nov 2000.
- [40] Muklesur Rahman, S. K. Kundu, B. K. Chaudhuri and A. Yoshizawa, "Frequency-Dependent Capacitance-Voltage Hysteresis in Ferroelectric Liquid Crystals: An Effect of the Frequency Dependence of Dielectric Biaxiality", *Journal of Applied Physics*, Vol. 98, 024114 (5 pp.), 2005.

- [41] Ciaran J. Brennan, "Characterization and Modeling of Thin-Film Ferroelectric Capacitors using C-V Analysis", *Integrated Ferroelectrics*, vol. 2, pp. 73-82, 1992.
- [42] H. Li, G. Subramanyam, and J. Wang, "Capacitance of Thin Ferroelectric Films Obtained with Different Methods," in *Proc. Symp Applications of Ferroelectrics* (ISAF 2008), vol. 1, pp. 1-3, 2008.
- [43] David Griffiths, *Introduction to Electrodynamics*, 3rd edition, prentice Hall, Inc., Upper Saddle River, NJ, 07458, 1999.
- [44] QQ Zhang, HLW Chan, CL Choy, "Dielectric and Pyroelectric Properties of P(VDF-TrFE) and PCLT-P(VDF-TrFE) 0-3 Nanocomposite Films", *Composites: Part A: Applied Science and Manufacturing*, Vol. 30, pp. 163-167, 1999.
- [45] D. Bolten, U. Bottger, and R. Waser, "Reversible and Irreversible Polarization Processes in Ferroelectric Ceramics and Thin Films", *Journal of Applied Physics*, Vol. 93, No. 3, pp. 1735-1742, 1 Feb 2003.
- [46] A. Ievlev, K. Verkhovskaya and V. Fridkin, "Landau-Khalatnikov Switching Kinetics in the Ferroelectric Copolymer Nanostructures", *Ferroelectric Letters*, Vol. 33, pp. 147-152, 2006.
- [47] Tae Kwon Song, "Landau-Khalatnikov Simulations for Ferroelectric Switching in Ferroelectric Random Access Memory Application", *Journal of the Korean Physical Society*, Vol. 46, No. 1, pp. 5-9, Jan 2005.
- [48] Somu Sivasubramanian, Allan Widom, and Yogendra Srivastava, "Equivalent Circuit and Simulations for the Landau-Khalatnikov Model of Ferroelectric Hysteresis", *IEEE Transactions on Ultrasonics, Ferroelectrics, and Frequency Control*, Vol. 50, No. 8, pp. 950-957, Aug 2003.

## Appendices

### Appendix A: Mathematical Derivation for Finding $\delta$ in S.L. Miller *et al.* Model

Expression for positive going branch of polarization hysteresis from S. L. Miller *et al.* model,

$$P_d^+(E) = P_s \tanh \left[ \frac{(E - E_C)}{2\delta} \right] \quad (A1)$$

The expression for  $\delta$  is predicted using the relation,  $P_d^+(0) = -P_R$ . So (A1) becomes,

$$-P_R = P_s \tanh \left[ \frac{-E_C}{2\delta} \right] \quad (A2)$$

From (A2),

$$\frac{E_C}{2\delta} = \tanh^{-1} \left( \frac{P_R}{P_s} \right) \quad (A3)$$

The formula for inverse hyperbolic tangent is given by,

$$\tanh^{-1}(Z) = \frac{1}{2} [\ln(1+Z) - \ln(1-Z)] \quad (A4)$$

From (A4),

$$\tanh^{-1}(Z) = \frac{1}{2} \left[ \ln \left( \frac{1+Z}{1-Z} \right) \right] \quad (A5)$$

(A3) can be written as,

$$\frac{E_C}{2\delta} = \frac{1}{2} \left[ \ln \left( \frac{1 + \cancel{P_R}/P_s}{1 - \cancel{P_R}/P_s} \right) \right] \quad (A6)$$

So the expression for  $\delta$  is,

## Appendix A (Continued)

$$\delta = E_C \left[ \ln \left( \frac{1 + P_R / P_S}{1 - P_R / P_S} \right) \right]^{-1} \quad (\text{A7})$$

## Appendix B: Mathematical Derivation to Find $\alpha$ and $\beta$ for Landau Free Energy Model for Monocrystalline Ferroelectrics

The expression electric field in terms of polarization is,

$$E(P) = -\alpha P + \beta P^3 \quad (\text{B1})$$

Equating (B1) to 0 gives the value of  $P_s$ .

$$-\alpha P_s + \beta P_s^3 = 0 \quad (\text{B2})$$

From (B2),

$$\pm P_s = \left( \frac{\alpha}{\beta} \right)^{1/2} \quad (\text{B3})$$

For maxima and minima, taking first derivative of (B1) with respect to P and equating to 0,

$$\frac{dE(P)}{dP} = -\alpha + 3\beta P^2 = 0 \quad (\text{B4})$$

From (B4),

$$P = \pm \left( \frac{\alpha}{3\beta} \right)^{1/2} \quad (\text{B5})$$

Taking second derivative of (B1) with respect to P,

$$\frac{d^2 E(P)}{dP^2} = 6\beta P \quad (\text{B6})$$

For positive value of P, (B6) is positive; so positive value of P from (B5) determines the minima. For negative value of P, (B6) is negative; so negative value of P from (B5) determines the maxima. The value of E at local minima and maxima gives the value of  $E_C$  which can be written as,

## Appendix B (Continued)

$$\pm E_c = -\alpha \left( \frac{\alpha}{3\beta} \right)^{1/2} + \beta \left( \frac{\alpha}{3\beta} \right)^{3/2} \quad (\text{B7})$$

From (B3),

$$\alpha = \beta P_s^2 \quad (\text{B8})$$

Using (B8) in (B7), for positive value of  $E_c$ ,

$$E_c = -\beta P_s^2 \left( \frac{\beta P_s^2}{3\beta} \right)^{1/2} + \beta \left( \frac{\beta P_s^2}{3\beta} \right)^{3/2} \quad (\text{B9})$$

From (B9),

$$E_c = -\frac{\beta P_s^3}{\sqrt{3}} + \frac{\beta P_s^3}{3\sqrt{3}} \quad (\text{B10})$$

and after solving (B10) for  $\beta$ ,

$$\beta = -\frac{3\sqrt{3}E_c}{2P_s^3} \quad (\text{B11})$$

Hence  $\alpha$  and  $\beta$  are calculated using (B8) and (B11).

## Appendix C: Mathematical Derivation to Find $\delta^+$ and $\delta^-$ for J. Yu *et al.* Model

Derivation of  $\delta^+$ :

Positive going polarization branch is expressed by

$$P_U = P_m^+ - (P_m^+ + P_{sat}^+) \left\{ \frac{1}{\pi} \tan^{-1} \left[ -\delta^+ (E_C^+ - E) \right] + \frac{1}{2} \right\} + \alpha^+ E \quad (C1)$$

When the applied electric field is zero, (C1) becomes,

$$P_R^- = P_m^+ - (P_m^+ + P_{sat}^+) \left\{ \frac{1}{\pi} \tan^{-1} \left[ -\delta^+ E_C^+ \right] + \frac{1}{2} \right\} + 0 \quad (C2)$$

From (C2),

$$(P_m^+ + P_{sat}^+) \left\{ \frac{1}{\pi} \tan^{-1} \left[ -\delta^+ E_C^+ \right] \right\} = P_m^+ - \frac{1}{2} (P_m^+ + P_{sat}^+) - P_R^- \quad (C3)$$

From (C3),

$$\tan^{-1} \left[ -\delta^+ E_C^+ \right] = \frac{\pi}{2} \left( \frac{P_m^+ - P_{sat}^+ - 2P_R^-}{P_m^+ + P_{sat}^+} \right) \quad (C4)$$

From (C4), the expression for  $\delta^+$  can be written as,

$$\delta^+ = - \frac{\tan \left[ \frac{\pi}{2} \left( \frac{P_m^+ - P_{sat}^+ - 2P_R^-}{P_m^+ + P_{sat}^+} \right) \right]}{E_C^+} \quad (C5)$$

Derivation of  $\delta^-$ :

Negative going polarization branch is expressed by

$$P_D = P_m^- - (P_m^- + P_{sat}^-) \left\{ \frac{1}{\pi} \tan^{-1} \left[ -\delta^- (E_C^- - E) \right] + \frac{1}{2} \right\} + \alpha^- E \quad (C6)$$

When the applied electric field is zero, (C6) becomes,

### Appendix C (Continued)

$$P_R^+ = P_m^- - (P_m^- + P_{sat}^-) \left\{ \frac{1}{\pi} \tan^{-1} [-\delta^- E_C^-] + \frac{1}{2} \right\} + 0 \quad (C7)$$

From (C7),

$$(P_m^- + P_{sat}^-) \left\{ \frac{1}{\pi} \tan^{-1} [-\delta^- E_C^-] \right\} = P_m^- - \frac{1}{2} (P_m^- + P_{sat}^-) - P_R^+ \quad (C8)$$

From (C8),

$$\tan^{-1} [-\delta^- E_C^-] = \frac{\pi}{2} \left( \frac{P_m^- - P_{sat}^- - 2P_R^+}{P_m^- + P_{sat}^-} \right) \quad (C9)$$

From (C9), the expression for  $\delta^-$  can be written as,

$$\delta^- = - \frac{\tan \left[ \frac{\pi}{2} \left( \frac{P_m^- - P_{sat}^- - 2P_R^+}{P_m^- + P_{sat}^-} \right) \right]}{E_C^-} \quad (C10)$$



## Appendix D: Mathematical Expression for Generating Negative Going Branch Polarization Curve Using Four-point Fit Model

The relation between  $P_{up}$  and  $P_{down}$  is given by,

$$P_{up} = -P_{down} \quad (D1)$$

$\alpha_{up}$  and  $\alpha_{down}$  are related as,

$$\alpha_{down} = (1 - \alpha_{up}) \quad (D2)$$

The expression for average polarization is given as,

$$P = \alpha_{up} P_{up} + \alpha_{down} P_{down} \quad (D3)$$

Using (D1), (D2) and (D3)

$$P = -(1 - \alpha_{down}) P_{down} + \alpha_{down} P_{down} \quad (D4)$$

From (D4),

$$P = -P_{down} + 2\alpha_{down} P_{down} \quad (D5)$$

From (D5),

$$P = (2\alpha_{down} - 1) P_{down} \quad (D6)$$

The value of coercive field ( $E_C$ ) and  $P_{down}$  are taken to be negative. The expression for  $X_j$  to find  $\alpha_{upj}$  is modified as follows.

$$X_j = \beta_1(E_j - E_C) + \beta_2(E_j - E_C)^2 u(E_j - E_C) + \beta_3(E_j - E_C)^2 u(E_C - E_j) + \beta_4(E_j - E_C)^3 \quad (D7)$$

Data for (3.2)-(3.5) evaluated at the four locations as shown in the following figure are summarized on the table below.

### Appendix D (Continued)

Table D.1: Values of the terms for calculating  $\beta_1$ ,  $\beta_2$ ,  $\beta_3$  and  $\beta_4$  for negative going polarization curve.

<b>j</b>	<b>E</b>	<b>P<sub>j</sub></b>	<b>r<sub>j</sub></b>	<b><math>\alpha_{upj}</math></b>	<b>X<sub>j</sub></b>
1	0	$7.29 \times 10^{-6} \text{ V/cm}^2$	-0.886	0.056	-5.55
2	$-E_C$	$8.0 \times 10^{-6} \text{ V/cm}^2$	-0.972	0.013	-23.01
3	$E_C(1+z)$	$-7.06 \times 10^{-6} \text{ V/cm}^2$	0.858	0.929	4.41
4	$E_C(1-z)$	$5.07 \times 10^{-6} \text{ V/cm}^2$	-0.617	0.191	-1.45

For the values of  $j= 1, 2, 3$  and  $4$ , (D7) yields three different equations which can be solved for the constants  $\beta_1, \beta_2, \beta_3$  and  $\beta_4$  using inverse matrix method as follows.

$$\begin{bmatrix} \beta_1 \\ \beta_2 \\ \beta_3 \\ \beta_4 \end{bmatrix} = M^{-1} \begin{bmatrix} X_1 \\ X_2 \\ X_3 \\ X_4 \end{bmatrix} = \begin{bmatrix} -1.89 \times 10^{-5} \text{ cm} / V \\ 3.66 \times 10^{-11} \text{ cm}^2 / V^2 \\ 3.20 \times 10^{-10} \text{ cm}^2 / V^2 \\ -4.79 \times 10^{-17} \text{ cm}^3 / V^3 \end{bmatrix} \quad (\text{D8})$$

where,

$$M = \begin{bmatrix} -E_C & (-E_C)^2 & 0 & (-E_C)^3 \\ -2E_C & (-2E_C)^2 & 0 & (-2E_C)^3 \\ zE_C & 0 & (zE_C)^2 & (zE_C)^3 \\ -zE_C & (-zE_C)^2 & 0 & (-zE_C)^3 \end{bmatrix} \quad (\text{D9})$$

Knowing the values of constants  $\beta_1, \beta_2, \beta_3$  and  $\beta_4$ , the negative going polarization curve can be plotted using (3.1).

## Appendix D (Continued)

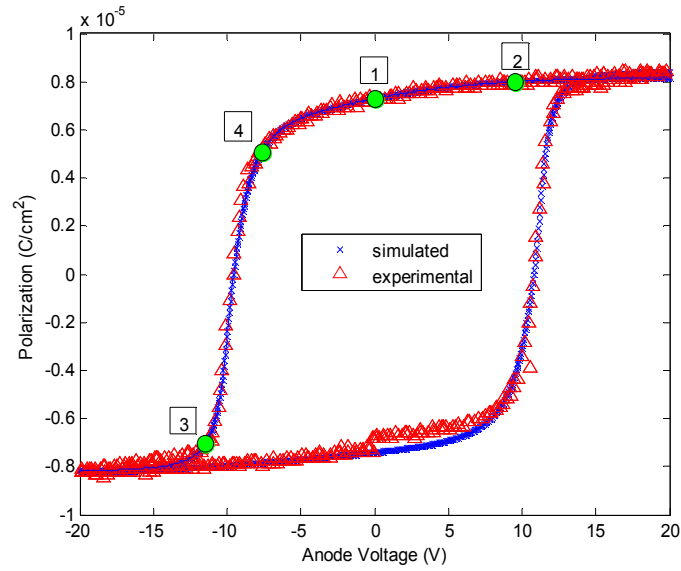


Figure D.1: Experimental and MATLAB simulated polarization hysteresis of ferroelectric by using new practical model with four-point fit on negative going curve.

## Appendix E: Mathematical Derivation for Small-Signal Capacitance

Rewriting (4.19),

$$-L \left[ \alpha \left( \frac{Q}{A} \right) + \beta \left( \frac{Q}{A} \right)^3 \right] + V = R_s \frac{dQ}{dt} \quad (F1)$$

Taking the derivative of above equation with respect to V,

$$-L \left[ \frac{\alpha}{A} \frac{dQ}{dV} + \frac{\beta}{A^3} \left( 3Q^2 \frac{dQ}{dV} \right) \right] + 1 = R_s \frac{d^2 Q}{dt dV} \quad (F2)$$

From (F2),

$$-L \frac{dQ}{dV} \left[ \frac{\alpha}{A} + \frac{3\beta Q^2}{A^3} \right] = R_s \frac{d^2 Q}{dt dV} - 1 \quad (F3)$$

From (F3),

$$\frac{dQ}{dV} = \frac{A^3 \left( 1 - R_s \frac{d^2 Q}{dt dV} \right)}{L \left( \alpha A^2 + 3\beta Q^2 \right)} \quad (F4)$$

From (F4),

$$C = \frac{dQ}{dV} = \frac{A \left( 1 - R_s \frac{d^2 Q}{dV dt} \right)}{L \left( \alpha + 3\beta Q^2 / A^2 \right)} \quad (F5)$$

Where,

$$\frac{A}{L \left( \alpha + 3\beta Q^2 / A^2 \right)} = C_{ideal} \quad (F6)$$

Applying  $\frac{d}{dt} = \omega$ , where  $\omega = 2\pi f$ , from (F5) and (F6), the expression for capacitance is,

$$C = \frac{dQ}{dV} = C_{ideal} - C_{ideal} R_s 2\pi f \frac{dQ}{dV} \quad (F7)$$

## Appendix E (Continued)

Solving for  $\frac{dQ}{dV}$  from (E7) we get,

$$C = \frac{dQ}{dV} = \frac{C_{ideal}}{1 + C_{ideal} R_s 2\pi f} \quad (F8)$$

The equation (F8) is the expression for small-signal capacitance of a ferroelectric capacitor where the dependence on the large-signal capacitance is explicit.

## Appendix F: MATLAB Code for Polarization Hysteresis Using S. L. Miller *et al.*

### Model

```
clc;
clear all;
close all;
format long;
load Expt2.dat; %Loads the experimental data
expt_vol = Expt2(:,1);
expt_pol = Expt2(:,2);
L=0.210e-4; % Length of the device in cm
Ec=4.847e5; % Expt coercive electric field in V/cm
Pr1=7.35e-6; % Expt Remnant polarization in C.cm^2
Pr=8.338e-6; % Modified Remnant polarization in C.cm^2
Ps=8.34e-6; % Spontaneous polarization in C.cm^2

V=[-20:4:20]; % External voltage range
[m,n]=size(V);
A = zeros(n,2);
B = zeros(n,2);
%E=V/L;
Prs1=Pr1/Ps;
Prs=Pr/Ps;
dlt1=Ec*(1/(log10((1+Prs1)/(1-Prs1)))); % Calculating delta for Sim1
dlt=Ec*(1/(log10((1+Prs)/(1-Prs)))); % Calculating delta for Sim2
for i=1:n
    E=V(i)/L; % Electric field
    Pd1=Ps*tanh((E-Ec)/(2*dlt1)); % Polarization for Sim1 curve
    Pd=Ps*tanh((E-Ec)/(2*dlt)); % Polarization for Sim2 curve
    Pdd1(i)=Pd1;
    A(i,1) = Pd;
    A(i,2) = V(i);
end;

plot(expt_vol,expt_pol,'^r');
hold on;
plot(A(:,2),Pdd1,'bo');
plot(A(:,2),A(:,1),'k*');
legend('Expt','Sim1','Sim2');
xlabel('Anode Voltage (V)');
ylabel('Polarization (C/cm^2)');
save file_data.dat;
Ec=-Ec;
```

## Appendix F (Continued)

```
dlt1=Ec*(1/(log10((1+Prs1)/(1-Prs1))));  
dlt=Ec*(1/(log10((1+Prs)/(1-Prs))));  
% Pd=Ps*tanh((E-Ec)/(2*dlt));  
V=[20:-0.4:-20];  
%V=[-20:0.2:20];  
  
for i=1:n  
    E=V(i)/L;  
    Pd1=Ps*tanh((E-Ec)/(2*dlt1));  
    Pd=Ps*tanh((E-Ec)/(2*dlt));  
    Pddd1(i)=-Pd1;  
    B(i,1) = -Pd;  
    B(i,2) = V(i);  
end;  
plot(expt_vol,expt_pol,'^r');  
plot(B(:,2),Pddd1,'bo');  
plot(B(:,2),B(:,1),'k*');  
hold on;
```

## Appendix G: Silvaco Code for Polarization and Capacitance Hysteresis Using S. L. Miller *et al.* Model

```
# Au MIM ferro Capacitor

go atlas
title Ferroelectric Capacitor

set cathode_thick=0.02
set ferro_thick = 0.21
set anode_thick = 0.02
set total_thick = $ferro_thick+$anode_thick
set dev_length = 500
set Ec = 0.4847e6

##### MESH SPECIFICATION

MESH width=100

X.MESH LOCATION=0.0      SPACING=10
X.MESH LOCATION=$dev_length  SPACING=10

y.mesh l=-$cathode_thick spacing=0.01
y.mesh l=0.0      spacing=0.01
y.mesh l=$ferro_thick  spacing=0.01
y.mesh l=$total_thick  spacing=0.01

##### MATERIALS
REGION num=1 user.MATERIAL=P(VDF-TrFE) x.min=0.0 x.max=$dev_length
y.min=0.0 y.max=$ferro_thick
#####

##### ELECTRODES
elect num=1 name=anode x.min=0 x.max=$dev_length y.min=-$cathode_thick
y.max=0.0 material=gold
elect num=2 name=cathode x.min=0 x.max=$dev_length y.min=$ferro_thick
y.max=$total_thick material=gold
#####

##### MATERIAL PARAMETERS
material region=1 user.group=insulator user.default=Si3N4 \
ferro.pr=7.35e-6 ferro.ps=8.34e-6 ferro.ec=$Ec ferro.eps=10
```



## Appendix G (Continued)

```
##### ELECTRODE PARAMETERS
# gold
contact name=anode workfunc=5.1
# gold
contact name=cathode workfunc=5.1
#####
##### DEVICE STRUCTURE
save outfile=MIS_ferro.str
tonyplot MIS_ferro.str
#####

##### MODEL AND DEFECT PARAMETERS
model reg=1 ferro print
#####

solve init
solve vanode=0
save outfile=MIS_ferro.str

method newton gummel itlimit=50 trap
log outfile=Simulation.log

probe polarization dir=90 x=250 y=0.11
probe permittivity dir=90 x=250 y=0.11

solve vfinal=20 vstep=0.4 name=anode ac freq=1e6 direct
material region=1 ferro.ec=-$Ec
solve vfinal=-20 vstep=-0.4 name=anode ac freq=1e6 direct
material region=1 ferro.ec=$Ec
solve vfinal=20 vstep=0.4 name=anode ac freq=1e6 direct

extract name="cap_den" curve(v."anode",c."anode""cathode") outfile="cap_den.dat"

tonyplot Simulation.log -overlay Experimental2.log -set polarization.set
tonyplot cap_den.dat
quit
```

## Appendix H: MATLAB Code for Polarization Hysteresis Using Landau Free Energy Model for Monocrystalline Ferroelectrics

```

clc;
format long;
close all;
clear all;
load Expt2.dat; % Loads the experimental data
expt_vol = Expt2(:,1);
expt_pol = Expt2(:,2);
Ps=6.8*10^-6; % Spontaneous polarization in C/cm^2 % 6.5*10^-2 C/m^2
ec=-4.847*10^5; % Coercive field in V/cm % -5*10^7 V/m
t=210; % P(VDF-TrFE) thickness in nm % 210*10^-7 cm
b=-((3*(3^(1/2))*ec)/(2*Ps^3)) % Beta (cm^5/(F*C^2))
a=b*Ps^2 % Alpha (cm/F)

V=20; % potential (V)
E=V/(t*10^(-7)); % Electric field (V/cm)

%%% finding cubic roots of b.P^3 - a.P = E comparing with
% x^3+a1.x^2+a2.x+a3=0 as in math hand book.
Q1=-(a/(3*b));
Q=round(Q1*1e20)/1e20; % Rounding Q1 to 20 decimal places
R1=E/(2*b);
R=round(R1*1e20)/1e20;
D=((Q).^3)+((R).^2);
S1=((((R)+(((Q).^3)+((R).^2)).^(1/2))).^(1/3));
S=round(S1*1e20)/1e20;
T1=((((R)-(((Q).^3)+((R).^2)).^(1/2))).^(1/3));
T=round(T1*1e20)/1e20;

p1=S+T; % First root
p2=-((0.5).*(S+T))+((S-T).*((3.^(1/2))./2).*i); % Second root
p3=-((0.5).*(S+T))-((S-T).*((3.^(1/2))./2).*i); % Third root

real1(1)=p1; % First root is always real
plot(expt_vol,expt_pol,'r^');
hold on;
plot(V, real1(1), '*');
hold on;
xlabel('Anode Voltage (V)');
ylabel('Polarization (C/cm^2)');
legend('Experimental','Simulated');

```

## Appendix H (Continued)

```

%%%%%%%%%%%%
n=((20+20)/.4)+1;
V=20:-0.4:-20;
% For selecting a root which is closest to the previous root
for m=2:n;
    E(m)=V(m)/(t*10^(-7));
    Q1=-(a/(3*b));
    Q=round(Q1*1e20)/1e20;
    R1=E(m)/(2*b);
    R=round(R1*1e20)/1e20;
    D=((Q).^3)+((R).^2);

    if (D>0 )

        if(D>0 && R1<0)
            S=(-abs((D).^(1/2)-abs(R)).^(1/3));
            T=(-abs((D).^(1/2)+abs(R)).^(1/3));
            p1=S+T;
            p2=-((0.5).*(S+T))+((S-T).*((3.^(1/2))./2).*i);
            p3=-((0.5).*(S+T))-((S-T).*((3.^(1/2))./2).*i);
            real1(m)=p1;
            plot(V(m), real1(m), '*');
            hold on;
        else
            S1=((R)+((((Q).^3)+((R).^2)).^(1/2))).^(1/3);
            S=round(S1*1e20)/1e20;
            T1=((R)-((((Q).^3)+((R).^2)).^(1/2))).^(1/3);
            T=round(T1*1e20)/1e20;
            p1=S+T;
            p2=-((0.5).*(S+T))+((S-T).*((3.^(1/2))./2).*i);
            p3=-((0.5).*(S+T))-((S-T).*((3.^(1/2))./2).*i);

            real1(m) = p1;

            plot(V(m), real1(m), '*');
            hold on;
        end;
    else
        S1=((R)+((((Q).^3)+((R).^2)).^(1/2))).^(1/3);
        S=round(S1*1e20)/1e20;
        T1=((R)-((((Q).^3)+((R).^2)).^(1/2))).^(1/3);
        T=round(T1*1e20)/1e20;

```

## Appendix H (Continued)

```

p1=S+T;
p2=-((0.5).*(S+T))+((S-T).*((3.^(1/2))./2).*i));
p3=-((0.5).*(S+T))-((S-T).*((3.^(1/2))./2).*i));
dist = [abs(real1(m-1)-p1) abs(real1(m-1)-p2) abs(real1(m-1)-p3)];
if (dist(1) < dist(2))
    small = p1;
    real1(m)=small;
    index = 1;
    plot(V(m),real1(m), '*');
    hold on;
else
    small = p2;
    real1(m)=small;
    index = 2;
    plot(V(m),real1(m), '*');
    hold on;
end
if(dist(3) < dist(index))
    small = p3;
    real1(m)=small;
    index = 3;
    plot(V(m),real1(m), '*');
    hold on;
end

end
end
plot(V,real1);
hold on;

%%% For another part of hysteresis loop

V=-20;
E=V/(t*10^(-7));
Q1=-(a/(3*b));
Q=round(Q1*1e20)/1e20; % Rounding Q1 to 20 decimal places
R1=E/(2*b);
R=round(R1*1e20)/1e20;
D=((Q).^3)+((R).^2);
S=(-abs((D).^(1/2)-abs(R)).^(1/3));
T=(-abs((D).^(1/2)+abs(R)).^(1/3));

```

## Appendix H (Continued)

```

p1=S+T;
p2=-((0.5).*(S+T))+((S-T).*((3.^(1/2))./2).*i);
p3=-((0.5).*(S+T))-((S-T).*((3.^(1/2))./2).*i);

real2(1)=p1;
plot(V, real2(1), '*');
hold on;
%%%%%%%%%%%%
n=((20+20)/.4)+1;
V=-20:0.4:20;
% For selecting a root which is closest to the previous root
for m=2:n
    E(m)=V(m)/(t*10^(-7));
    Q1=-(a/(3*b));
    Q=round(Q1*1e20)/1e20;
    R1=E(m)/(2*b);
    R=round(R1*1e20)/1e20;
    D=((Q).^3)+((R).^2);

    if (D>0 )

        if(D>0 && R1<0)
            S=(-abs((D).^(1/2))-abs(R)).^(1/3));
            T=(-abs((D).^(1/2))+abs(R)).^(1/3));
            p1=S+T;
            p2=-((0.5).*(S+T))+((S-T).*((3.^(1/2))./2).*i);
            p3=-((0.5).*(S+T))-((S-T).*((3.^(1/2))./2).*i);
            real2(m)=p1;
            plot(V(m), real2(m), '*');
            hold on;
        else
            S1=(((R)+(((Q).^3)+((R).^2)).^(1/2))).^(1/3));
            S=round(S1*1e20)/1e20;
            T1=(((R)-(((Q).^3)+((R).^2)).^(1/2))).^(1/3));
            T=round(T1*1e20)/1e20;
            p1=S+T;
            p2=-((0.5).*(S+T))+((S-T).*((3.^(1/2))./2).*i);
            p3=-((0.5).*(S+T))-((S-T).*((3.^(1/2))./2).*i);

            real2(m) = p1;

            plot(V(m), real2(m), '*');

```

## Appendix H (Continued)

```
        hold on;
    end;
else
    S1=(((R)+((((Q).^3)+((R).^2)).^(1/2))).^(1/3));
    S=round(S1*1e20)/1e20;
    T1=(((R)-((((Q).^3)+((R).^2)).^(1/2))).^(1/3));
    T=round(T1*1e20)/1e20;
    p1=S+T;
    p2=-((0.5).*(S+T))+((S-T).*((3.^(1/2))./2).*i);
    p3=-((0.5).*(S+T))-((S-T).*((3.^(1/2))./2).*i);
    dist = [abs(real2(m-1)-p1) abs(real2(m-1)-p2) abs(real2(m-1)-p3)];
    if (dist(1) < dist(2))
        small = p1;
        real2(m)=small;
        index = 1;
        plot(V(m),real2(m), '*');
        hold on;
    else
        small = p2;
        real2(m)=small;
        index = 2;
        plot(V(m),real2(m), '*');
        hold on;
    end
    if(dist(3) < dist(index))
        small = p3;
        real2(m)=small;
        index = 3;
        plot(V(m),real2(m), '*');
        hold on;
    end
end
end
plot(V,real2);
hold on;
```

## Appendix I: MATLAB Code for Polarization Hysteresis Using J. Yu *et al.* Model

```
clc;
clear all;
close all;
%%%%%loading experimental data
format long;
load Expt2.dat;
expt_vol = Expt2(:,1);
expt_pol = Expt2(:,2);
%%%%%%%%%

ecp=(5.145e5)*(1e2); %V/m positive coercive field
ecn=-(4.549e5)*(1e2); %V/m negative coercive field
%t=210; %thickness in nm
T=210e-9; % thickness in m

pmaxp=(8.461*10^-6)*(1*10^4); %C/m^2 maximum positive polarization
pmaxn=-(8.2274*10^-6)*(1*10^4); %C/m^2 maximum negative polarization
psatp=(8.461*10^-6)*(1*10^4); %C/m^2 positive saturation polarization
psatn=-(8.2274*10^-6)*(1*10^4); %C/m^2 negative saturation polarization
prp=(7.29*10^-6)*(1*10^4); %C/m^2 positive remnant polarization
prn=-(7.41*10^-6)*(1*10^4); %C/m^2 negative remnant polarization

vmaxp=20; %maximum positive applied voltage in volt
vmaxn=-20; %maximum negative applied voltage in volt
emaxp=vmaxp/T; %maximum positive electric field in v/m
emaxn=vmaxn/T; %maximum negative electric field in v/m
ap=(pmaxp-psatp)/emaxp %alpha+
an=(pmaxn-psatn)/emaxn %alpha-

%for calculating delta+
x=((pmaxp-(2*prn)-psatp)/(pmaxp+psatp));
ddp=-(tan(x*(pi/2))/ecp) %delta+

%for calculating delta-
z=((pmaxn-(2*prp)-psatn)/(pmaxn+psatn));
ddn=-(tan(z*(pi/2))/ecn) %delta-

n=((vmaxp-vmaxn)/.2)+1;
%for positive sweep
V=vmaxn:0.2:vmaxp;
for m=1:n
    E(m)=V(m)./T;
```

## Appendix I (Continued)

```
y(m)=-(ddp.*(ecp-E(m)));
PDUP(m)=pmaxp-((pmaxp+psatp).*((atan(y(m))./pi)+0.5))+(ap.*E(m));
PP(m)=PDUP(m)*1e-4; %polarization in C/cm2
end;
plot(expt_vol,expt_pol,'r^');
hold on;
plot(V, PP,'b*')
legend('Experimental','Simulated');
%for negative sweep
VV=vmaxp:-0.2:vmaxn;
for m=1:n
    EE(m)=VV(m)./T;
    yy(m)=-(ddn.*(ecn-EE(m)));
    PDDN(m)=pmaxn-((pmaxn+psatn).*((atan(yy(m))./pi)+0.5))+(an.*EE(m));
    PPPP(m)=PDDN(m)*1e-4; %polarization in C/cm2
end;
plot(VV, PPPP,'b*')
hold on;
xlabel('Voltage (V)');
ylabel('Polarization (C/cm^2)');
```



## Appendix J: MATLAB Code for Polarization Hysteresis Using Y. L. Wang *et al.*

### Model

```
clc;
clear all;
close all;

%%%%%%%%
format long;
load Expt2.dat;
expt_vol = Expt2(:,1);
expt_pol = Expt2(:,2);
%%%%%%%%

B1=1.2*10^-7; %1.622*(3.1407e-6)*1.89e-2; %m/V % increase this to get more steep
curve
B2=-4.357*10^-25; %-6.4534e-20*(1.89e-2)^3; % m^3/V^3,

eps_ferro=10;
PR=(7.35*10^-6)*(1*10^4); %C/m^2 % if decreased, polarization constant/ extreme
decrease in capacitance (desired)
%Ps=7e-6 % C/cm^2
PS=(8.34*10^-6)*(1*10^4); %C/m^2 % if increased, polarization constant/ small
increase in capacitance
%Ec=0.5e6 %V/cm
EC=(0.4847*10^6)*(1*10^2); %V/m % if increased, thickness of polarization curve
increases/ slight decrease in capacitance
%t=210; %thickness in nm
T=210*10^-9; % thickness in m
%fer_area = 500e-4*100e-4; % AREA in cm^2
fer_area = 5e-4*1e-4; % AREA in m^2
% calculation of delta (for capacitance)
Prs=PR/PS;
dlt=EC*(1/(log10((1+Prs)/(1-Prs))));

% for calc of a
tpc=27; %room temp in centigrade
tp=300; % in kelvin
t0c=170; %Curie Weiss temp in centigrade
t0=443; % Curie Weiss temp in kelvin
C=500; %Curie Weiss constant in Kelvin
ee0=8.8541e-12; %permittivity of free space (F/m)
a=-((tp-t0)/(ee0*C)); % alfa (m/F), should be negative and without
```

## Appendix J (Continued)

```

%factor '2'(as in original formula) to compensate the change in formula
b=4.1e12; % beta ( $m^5/(F \cdot C^2)$ )(directly choosen)
%increases in this value decreases height of hysteresis
V0=20;
E0=V0/T;
aupp=(atan((B1.*(E0-EC)))+(B2.*(E0-EC).^3))+(pi./2))./pi
aupn=(atan((B1.*(-E0-EC)))+(B2.*(-E0-EC).^3))+(pi./2))./pi

n=((V0+V0)/.4)+1;
V=V0:-0.4:-V0;
for m=1:n
    E(m)=V(m)./T;
    aup(m)=(atan((B1.*(E(m)-EC)))+(B2.*(E(m)-EC).^3))+(pi./2))./pi;
    baup(m)=aup(m)+((1-aupp-aupn)/2); %alfa up prime
    p3 = [b 0 -a (1-(2.*baup(m))).*E(m)];
    r3 = roots(p3) ;
    Pup(m) = abs(r3(1));
    P(m)=((2.*baup(m))-1).*Pup(m); %in C/m2
    PP(m)=P(m)*1e-4; % in C/cm2
    Pa(m)=((2.*aup(m))-1).*Pup(m); %in C/m2
    PPa(m)=Pa(m)*1e-4; % in C/cm2
    %above part is for for calculating polarization

    eps(m)=eps_ferro+(((PS-(P(m).^2)./PS))./(2.*dlt.*ee0));
    cap_ferr(m)= ((eps(m).*ee0)*fer_area)./T;
    FP(m)=-P(m); % flipping polarization value in C/m2
    FPP(m)=-PP(m); % flipping polarization value in C/cm2
    FPPa(m)=-PPa(m);
    hold on;
end;

figure (1)
%plot (V, PPa,'b.','MarkerSize',10)
plot (V, PPa,'b. ');
plot (V, PP,'kx')
plot(expt_vol,expt_pol,'r^');
plot(V, Pup*1e-4, 'g*')
legend( 'Using \alpha_u_p','Using \alpha^I_u_p','Experimental','P_u_p');
figure (2)
plot(V, aup,'k')
hold on;

```

## Appendix J (Continued)

```

plot(V, baup)
%%%%%%%%%%%%%%%%%%%%%%%%%%%%%%%%%%%%%%%%%%%%%%%%%%%%%%%%%%%%%%%%%%%%%%%%

VV=-V0:0.4:V0;
for m=1:n
    eps(m)=eps_ferro+(((PS-(FP(m).^2)./PS))./(2.*dlt.*ee0));
    cap_ferr2(m)= ((eps(m).*ee0)*fer_area)./T;
    hold on;
end;

figure (1)

plot (VV, FPP,'kx');
plot (VV, FPPa,'b. ');
hold on;
xlabel('Anode Voltage (V)');
ylabel('Polarization (C/cm^2)');
box on;

axis([-20 20 -1e-5 1e-5])

h1 = figure(1);
h2 = get(h1,'CurrentAxes');
% Note: edit these numbers to change position
% and size of inset plot
h3 = axes('pos',[.757 .16 .15 .2]);
plot (V, PP,'kx','MarkerSize',5)
hold on
plot (V, PPa,'O','MarkerEdgeColor','b','MarkerFaceColor','b','MarkerSize',2);
hold on
plot (VV, FPP,'kx','MarkerSize',5)
hold on
plot (VV, FPPa,'O','MarkerEdgeColor','b','MarkerFaceColor','b','MarkerSize',2);
hold on
% xlabel('V')
% ylabel('P')
axis([15.8 20.1 0.72e-5 0.88e-5])

```

## Appendix K: MATLAB Code for Polarization and Capacitance Hysteresis Using Model Based on Predicting Coefficients $\beta_1$ and $\beta_2$

```

clc;
clear all;
close all;

%%%%%
format long;
load Expt2.dat;
expt_vol = Expt2(:,1);
expt_pol = Expt2(:,2);
%%%%%%%%%%

area=5e-4*1e-4; % AREA in m^2 %
eps_ferro=10; % Relative permittivity of P(VDF-TrFE)
ee0=8.8541e-12; % permittivity of free space (F/m)
%t=210; %thickness in nm
T=210e-9; % thickness in m
Cc=(area*ee0*eps_ferro)/T; % Capacitance
EC=(4.847e5)*(1e2); %V/m

% For calculating beta1 and beta2
PRneg=-(7.35*10^-6)*(1*10^4); %C/m^2 negative remnant polarization
PC=-(7.994*10^-6)*(1*10^4); %C/m^2 Polarization at negative coercive field
PUP=(8.34*10^-6)*(1*10^4); %C/m^2 Spontaneous polarization
r1=PRneg/PUP
r2=PC/PUP
aup1=(1+r1)/2
aup2=(1+r2)/2
x1=-tan(pi*(aup1-0.5))
x2=-(tan(pi*(aup2-0.5)))/2
B2=(x2-x1)/(3*EC^3)
B1=((4*x1)-x2)/(3*EC)

pvec= [PC PRneg ]/(1*10^4);
Vvec=[ -T*EC 0 ];

V0=20;
E0=V0/T;
aupp=(atan((B1.*(E0-EC))+(B2.*(E0-EC).^3))+(pi./2))./pi;
aupn=(atan((B1.*(-E0-EC))+(B2.*(-E0-EC).^3))+(pi./2))./pi;
k=((1-aupp-aupn)./2);

```

## Appendix K (Continued)

```

n=((V0+V0)/.05)+1;
V=V0:-0.05:-V0;
for m=1:n
    E(m)=V(m)./T;
    x(m)=(B1.*(E(m)-EC))+(B2.*(E(m)-EC).^3);
    aup(m)=(atan(x(m))+(pi./2))./pi; % alpha up
    baup(m)=aup(m)+k; % alpha up prime
    %P(m)=((2.*baup(m))-1).*PUP; % in C/m2
    P(m)=((2.*aup(m))-1).*PUP; % in C/m2
    PP(m)=P(m)*1e-4; % in C/cm2
    %plot (V(m), PP(m),'b*')
    FP(m)=-PP(m); % flipping polarization value

    %for capacitance
    xx(m)=1./(1+(x(m).^2));
    y(m)=B1+(3.*B2.*((E(m)-EC).^2));
    daupdv(m)=(xx(m).*y(m))./(pi.*T);
    C(m)=Cc+(2.*area.*PUP.*daupdv(m));
    hold on;
end;
figure(1); % Polarization plot
plot(expt_vol,expt_pol,'r^');
plot (V, PP,'bx')

plot( Vvec, pvec,'O','MarkerEdgeColor','k','MarkerFaceColor','g','MarkerSize',11);
hold on;

xlabel('Anode Voltage (V)');
ylabel('Polarization (C/cm^2)');
box on;
VV=-V0:0.05:V0;
figure(1); % Polarization plot
plot (VV, FP,'bx')
hold on;
legend( 'Experimental','Simulated');

figure(2); % Capacitance plot
plot(V,C,'g*');
hold on;
plot(VV,C,'g*');
xlabel('Voltage (V)');
ylabel('capacitance (F)');

```

## Appendix L: MATLAB Code for Polarization Hysteresis Using New Practical Model with Three-point Fit

```

clc;
clear all;
close all;
n1=3;% exponent for u term in expression
n2=5;

%%%%%%%%
format long;
load Expt2.dat;
expt_vol = Expt2(:,1);
expt_pol = Expt2(:,2);
%%%%%%%%

Vo=20;

%Ec=-0.5e6 %V/cm
EC=(4.847e5)*(1e2); %V/m
z=0.2 % E3=EC(1+z)
% new model based on recognition there is no perfect cubic symmetry respect to Ec
%t=210; %thickness in nm
T=210e-9; % thickness in m
Vcon=(1+z)*EC*T

% use two values but on negative side of Ec
PRneg=-(7.35*10^-6)*(1*10^4); %C/m^2 negative remnant polarization
PC=-(7.994*10^-6)*(1*10^4); %C/m^2 polarization at negative coercive field
P3=(7.15*10^-6)*(1*10^4); %C/m^2 polarization at V3 ( using z factor)
PUP=(8.34*10^-6)*(1*10^4); %C/m^2 Pmax or Ps

% for calculation B1, B2, B3
r1=PRneg/PUP
r2=PC/PUP
r3=P3/PUP
pvec= [PC PRneg P3 ]/(1*10^4);
Vvec=[ -T*EC 0 T*EC*(1+z) ];
aup1=(1+r1)/2
aup2=(1+r2)/2
aup3=(1+r3)/2
x1=tan(pi*(aup1-0.5))% at zero
x2=tan(pi*(aup2-0.5)) % at -EC

```

## Appendix L (Continued)

```

x3=tan(pi*(aup3-0.5)) % at +EC(1+z)

Vmax=Vo;
Vmin=-Vo;
N=900;
stair=0:N; % sequence starts at zero and ends on N
une=ones(size(stair));
V=Vmin*une+ (Vmax-Vmin)/N*stair; % allowed values for V
Efield=V/T; % allowed electric field values

% x= B1*(EFIELD -EC)+ B2* u(EFIELD -EC)*(EFIELD -EC)^n1 +B3*(EFIELD -
EC)^n2
%Efield=0;
%x1= -EC* B1 + 0 + B3*(-EC)^n2
%Efield=-EC;
%x2= - 2*B1*EC + 0 + B3*(-2*EC)^n2 ;
% EFIELD= EC(1+z)
%x3= z* B1*EC + B2*(z*EC)^n1 + B3*(z*EC)^n2
%%%%%%%%%%%%%%

a=-EC; b=0; c=(-EC)^n2;
d=-2*EC; e=0; f=(-2*EC)^n2;
g=z*EC; h=(z*EC)^n1; k=(z*EC)^n2;
% invers matrix coefficients
A=e*k-f*h; D= c*h-b*k; G=b*f-c*e;
B=f*g-d*k; E= a*k-c*g; H=c*d-a*f;
C=d*h-e*g; F=g*b-a*h; K=a*e-b*d
% detA in denominator is not yet included
detA=a*A+b*B+c*C;
B1=(A*x1+D*x2+G*x3)/detA% predicted constant
B2=(B*x1+E*x2+H*x3)/detA% predicted constant
B3=(C*x1+F*x2+K*x3)/detA% predicted constant

text1=num2str( n1)
text2=num2str( n2)
Gtext=strcat( 'exponents unit step and for extra power term ', text1, ', ', text2)

u= 0.5*( (sign(Efield-(EC)*une))+une); % unit step function

x=B1*(Efield-EC*une)+ B2*u.*(Efield-EC*une).^(n1*une)+ B3*(Efield -
EC*une).^(n2*une)

```

## Appendix L (Continued)

```
% predict Xarray values and alpha_up
aup= (atan(x)+une*pi/2)/pi;
P=(2*aup-une)*PUP;
PP=P*1e-4; % in C/cm2
plot(expt_vol,expt_pol,'r^');
hold on;
for m=1:N+1
    plot(V(m), PP(m),'bx')
    FP(m)=-PP(m); % flipping polarization value
    hold on;
end;

legend('Experimental','Simulated');
xlabel('Anode Voltage (V)');
ylabel('Polarization (C/cm^2)');

for m=1:N+1
    VV(m)=V(N+2-m);
    hold on;
end;
plot(VV, FP,'bx')
hold on;
plot(V, PP, Vvec, pvec,'O','MarkerEdgeColor','k','MarkerFaceColor','g','MarkerSize',10);
```



## Appendix M: MATLAB Code for Polarization and Capacitance Hysteresis Using New Practical Model with Four-point Fit

```

clc;clear all;close all;
%%%%%
format long;
load Expt2.dat;
expt_vol = Expt2(:,1);
expt_pol = Expt2(:,2);
%%%%%%%%%%
area=5*10^-8; % AREA in m^2 %
eps_ferro=10; % Relative permittivity of P(VDF-TrFE)
ee0=8.8541e-12; %permittivity of free space (F/m)
%t=210; %thickness in nm
T=210e-9; % thickness in m
Cc=(area*ee0*eps_ferro)/T; % For total capacitance calculation

%%%%%%%%%positive sweep
EC=(5.145e5)*(1e2); %V/m coercieve field
z=0.2 % E3=EC(1+z)
z4=0.2 % E3=EC(1+z4)
Vcon=(1+z)*EC*T
Vconneg=(1-z4)*EC*T
PRneg=(-7.41*10^-6)*(1*10^4); %C/m^2 negative remnant polarization
PC=(-7.994*10^-6)*(1*10^4); %C/m^2 polarization at negative coercieve field
P3=(7.68*10^-6)*(1*10^4); %C/m^2 polarization at V3 at Vcon
P4=(-5.42*10^-6)*(1*10^4); %C/m^2 polarization at V4 at Vconneg
PUP=(8.460834961*10^-6)*(1*10^4); %C/m^2 max pol or spontaneous pol
pvec= [PC PRneg P3 P4 ]/(1*10^4);
Vvec=[ -T*EC 0 T*EC*(1+z) T*EC*(1-z4) ];
% for calculation B1, B2, B3
r1=PRneg/PUP
r2=PC/PUP
r3=P3/PUP
r4=P4/PUP

aup1=(1+r1)/2
aup2=(1+r2)/2
aup3=(1+r3)/2
aup4=(1+r4)/2

x1=tan(pi*(aup1-0.5))
x2=tan(pi*(aup2-0.5))

```

## Appendix M (Continued)

```

x3=tan(pi*(aup3-0.5))
x4=tan(pi*(aup4-0.5))
% calculating B1, B2,B3,B4 using matrix inversion method using inv function
% x= B1*(EFIELD -EC)+ B2*(EFIELD -EC)^2* u( E-EC) + B3*(EFIELD-EC)^2
u(EC-E) + B4*(EFIELD -EC)^3

%EFIELD=0;
%x1= -EC* B1 + B2*0 B3*(-EC)^2) + B4*(0-EC)^3
%EFIELD=-EC;
%x2= - 2*B1*EC + B2*0 B3*(-2*EC)^2) + B4*(-2*EC)^3 ;
% EFIELD= EC(1+z)
%x3= z* B1*EC + B2*(z*EC)^2 + B3*0 + B4*(z*EC)^3
% EFIELD= EC(1-z)
%x4= -z* B1*EC + B2*0 + B3*(-z*EC)^2 + B4*(-z*EC)^3
%%%%%%%%%%%%%%

A=[-EC 0 (-EC)^2 (-EC)^3;
-(2*EC) 0 (-2*EC)^2 (-2*EC)^3 ;
z*EC (z*EC)^2 0 (z*EC)^3;
-z4*EC 0 (-z4*EC)^2 (-z4*EC)^3];
I=inv(A)
X=[x1; x2; x3; x4]

B=I*X
B1=B(1)
B2=B(2)
B3=B(3)
B4=B(4)
%%%%%%%%%%
Vo=20;
Vmax=Vo;
Vmin=-Vo;
N=1000;
stair=0:N; % sequence starts at zero and ends on N
une=ones(size(stair));
V=Vmin*une+ (Vmax-Vmin)/N*stair; % allowed values for V
Efield=V/T; % allowed electric field values
up= 0.5*( (sign(Efield-EC*une))+une);
um=0.5*( (sign(EC*une-Efield))+une);

x= B1*(Efield-EC)+ B2*(Efield -EC).^ (2*une). *up + B3*(Efield-EC).^ (2*une). *um +
B4*(Efield -EC).^ (3*une);

```

## Appendix M (Continued)

```

aup= (atan(x)+une*pi/2)/pi;
P=(2*aup-une)*PUP;
PP=P*1e-4; % in C/cm2
figure(1);
plot( V, PP, 'x')
hold on;
plot(expt_vol,expt_pol,'r^');
hold on;
plot( V, PP, Vvec, pvec,'O','MarkerEdgeColor','k','MarkerFaceColor','g','MarkerSize',10);

for m=1:N+1
    %for capacitance
    xx(m)=1./(1+(x(m).^2));
    y(m)=B1+(2.*B2.*((Efield(m)-EC).*up(m)))+(2.*B3.*((Efield(m)-
EC).*um(m)))+(3.*B4.*((Efield(m)-EC).^2));
    daupdv(m)=(xx(m).*y(m))./(pi.*T);
    C(m)=Cc+(2.*area.*PUP.*daupdv(m));
end;
figure(2); %capacitance plot
plot(V,C,'bx');
hold on;
xlabel('Voltage (V)');
ylabel('capacitance (F)');

%%%%%%%% for down sweep part
ECN=-(4.549e5)*(1e2); %V/m negative coercieve electric field
z=0.2 % E3=ECN(1+z)
z4=0.2 % E3=ECN(1+z4)
%t=210; %thickness in nm
T=210e-9; % thickness in m
Vcon=(1+z)*ECN*T %v3
Vconneg=(1-z4)*ECN*T %v4
PRpos=(7.2938*10^-6)*(1*10^4); %C/m^2 positive remnant polarization
PC=(8.0*10^-6)*(1*10^4); %C/m^2 polarization at positive coercieve field
P3=-(7.06042*10^-6)*(1*10^4); %C/m^2 polarization at V3 at Vcon
P4=(5.0765*10^-6)*(1*10^4); %C/m^2 polarization at V4 at Vconneg
PUP=-(8.22743*10^-6)*(1*10^4); %C/m^2 max pol or spontaneous pol
pvec= [PC PRpos P3 P4 ]/(1*10^4);
Vvec=[ -T*ECN 0 T*(ECN)*(1+z) T*(ECN)*(1-z4) ];

r1=PRpos/PUP
r2=PC/PUP

```

## Appendix M (Continued)

```

r3=P3/PUP
r4=P4/PUP

aup1=(1+r1)/2
aup2=(1+r2)/2
aup3=(1+r3)/2
aup4=(1+r4)/2

x1=tan(pi*(aup1-0.5))
x2=tan(pi*(aup2-0.5))
x3=tan(pi*(aup3-0.5))
x4=tan(pi*(aup4-0.5))
% calculating B1, B2,B3,B4 using matrix inversion method using inv function
% x= B1*(EFIELD -ECN)+ B2*(EFIELD -ECN)^2* u( E-ECN) + B3*(EFIELD-
ECN)^2 u(ECN-E) + B4*(EFIELD -ECN)^3

%EFIELD=0;
%x1= -ECN* B1 + B2*(-ECN)^2 B3*0 + B4*(0-ECN)^3
%EFIELD=-ECN;
%x2= - 2*B1*ECN + B2*(-2*ECN)^2 B3*0 + B4*(-2*ECN)^3 ;
% EFIELD= ECN(1+z)
%x3= z* B1*ECN + B2*0 + B3*(z*ECN)^2 + B4*(z*ECN)^3
% EFIELD= ECN(1-z)
%x4= -z* B1*ECN + B2*(-z*ECN)^2 + B3*0 + B4*(-z*ECN)^3
%%%%%%%%%%%%%%

A=[-ECN (-ECN)^2 0 (-ECN)^3;
-(2*ECN) (-2*ECN)^2 0 (-2*ECN)^3 ;
z*ECN 0 (z*ECN)^2 (z*ECN)^3;
-z4*ECN (-z4*ECN)^2 0 (-z4*ECN)^3];
I=inv(A)
X=[x1; x2; x3; x4]

B=I*X
B1=B(1)
B2=B(2)
B3=B(3)
B4=B(4)
%%%%%%%%%%
Vo=20;
Vmax=Vo;
Vmin=-Vo;

```

## Appendix M (Continued)

```

N=1000;
stair=0:N; % sequence starts at zero and ends on N
une=ones(size(stair));
V=Vmin*une+ (Vmax-Vmin)/N*stair; % allowed values for V
Efield=V/T; % allowed electric field values
up= 0.5*( (sign(Efield-ECN*une))+une);
um=0.5*( (sign(ECN*une-Efield))+une);

x= B1*(Efield-ECN)+ B2*(Efield -ECN).^(2*une).*up + B3*(Efield-
ECN).^(2*une).*um + B4*(Efield -ECN).^(3*une);
aup= (atan(x)+une*pi/2)/pi;
P=(2*aup-une)*PUP;
PP=P*1e-4; % in C/cm2
figure(1);
plot( V, PP, 'x')
hold on;
plot(expt_vol,expt_pol,'r^');
hold on;
plot( V, PP, Vvec, pvec,'O','MarkerEdgeColor','k','MarkerFaceColor','g','MarkerSize',10);
%plot( V, PP, Vvec, pvec,'s');
legend( 'simulated','experimental');
xlabel('Anode Voltage (V)');
ylabel('Polarization (C/cm^2)');

for m=1:N+1
    %for capacitance
    xx(m)=1./(1+(x(m).^2));
    y(m)=B1+(2.*B2.*((Efield(m)-ECN).*up(m)))+(2.*B3.*((Efield(m)-
ECN).*um(m)))+(3.*B4.*((Efield(m)-ECN).^2));
    daupdv(m)=(xx(m).*y(m))./(pi.*T);
    C(m)=Cc+(2.*area.*PUP.*daupdv(m));
end;
figure(2); %capacitance plot
plot(V,C,'bx');
hold on;
xlabel('Anode Voltage (V)');
ylabel('capacitance (F)');

```

## Appendix N: MATLAB Code for Large-Signal Capacitance Hysteresis Using Point to Point Numerical Derivative

```
clc;clear all;close all;
%%%%%
format long;
load Expt2.dat;
expt_vol = Expt2(:,1);
expt_pol = Expt2(:,2);
%%%%%%%%%
format long;
load Expt2nega.dat;
expt_vol1 = Expt2nega(:,1);
expt_pol1 = Expt2nega(:,2);
load Expcapa1.dat;
expv=Expcapa1(:,1);
expc=Expcapa1(:,2);
load Expt2pos.dat;
exptposvol = Expt2pos(:,1);
exptpospol = Expt2pos(:,2);
%%%%%%%%%

areacgs=5e-4
eps_ferro=10; % Relative Permittivity of P(VDF-TrFE)
ee0=8.8541e-12; % permittivity of free space (F/m)
ee0cgs=8.8541e-14;
%t=210; %thickness in nm
T=210e-9; % thickness in m
Tcgs=210e-7;

%%%%% jumping points
jump=3;
R=rem (251, (jump+1));
N=1+((251-R)/(jump+1));

rmexptv(1)= expt_vol1(1);
rmexptp(1)= expt_pol1(1);
for n=1:1:(N-1)
    rmexptv(n+1)= expt_vol1(1+(jump+1).*n);
    rmexptp(n+1)= expt_pol1(1+(jump+1).*n);
end;

derN= diff(rmexptp)./diff(rmexptv);
```

## Appendix N (Continued)

```
derNN=round(derN.*1e40)./1e40;
for n=1:(N-1)
    exptnegV(n)= rmexptv(n);
    Cnumneg(n) = (areacgs/Tcgs).*((ee0cgs*eps_ferro)+(Tcgs*derNN(n)));
end
%%positive part
for j=1:251
    exptposvol2(j)= exptposvol(252-j);
    exptpospola2(j) = exptpospola(252-j);
end;
%%removing two points
    rmexptvp(1)= exptposvol2(1);
    rmexptpp(1)= exptpospola2(1);
    for n=1:1:(N-1)
        rmexptvp(n+1)= exptposvol2(1+(jump+1).*n);
        rmexptpp(n+1)= exptpospola2(1+(jump+1).*n);
    end;
derP= diff(rmexptpp)./diff(rmexptvp);
derPP=round(derP.*1e40)./1e40;

for n=1:(N-1)
    exptposV(n)= rmexptvp(n);
    Cnumpos(n) = (areacgs/Tcgs).*((ee0cgs*eps_ferro)+(Tcgs*derPP(n)));
end

figure(1); %%capacitance plot
plot(exptnegV, Cnumneg, 'k', 'linewidth', 2.5 );
hold on;
plot(exptposV, Cnumpos, 'r', 'linewidth', 2.5 );
legend ('Num-der-neg-sweep', 'Num-der-pos-sweep');
xlabel('Voltage (V)');
ylabel('capacitance (F)');
```

## Appendix O: MATLAB Code for Capacitance Hysteresis Using S. L. Miller *et al.*

### Model

```
clear all;close all; clc;
L=0.210e-4;    % Thickness of the device in cm
Ec=4.847e5;    % Coercive field (V/cm)
Pr=7.35e-6;    % Remnant Polarization (C/cm^2)
Ps=8.34e-6;    % Spontaneous Polarization (C/cm^2)
eps_ferro=10;  % Relative permittivity of P(VDF-TrFE)
epso=8.854e-14; % Permittivity of free space (F/cm)
V=[-20:4:20];
[m,n]=size(V);
A = zeros(n,2);
B = zeros(n,2);
eps_E=zeros(n,2);
cap_den=zeros(n,2);
fer_area = 500e-4*100e-4; % AREA
Prs=Pr/Ps;
dlt=Ec*(1/(log10((1+Prs)/(1-Prs)))); % Delta
for i=1:n
    E=V(i)/L;
    %eps_E=eps_ferro+(Ps*2*dlt*(sech((E-Ec)/(2*dlt)))^2);
    % Field dependent permittivity
    eps_E=epso*eps_ferro+(Ps*(sech((E-Ec)/(2*dlt)))^2)/(2*dlt);
    cap_ferr= (eps_E*fer_area)/L;
    cap_den(i,2) = cap_ferr
    cap_den(i,1) = V(i)
end
figure(1);
plot(cap_den(:,1), cap_den(:,2),'-b');
hold on;
V=[-20:4:20];
Ec=-Ec;
for i=1:n
    E=V(i)/L;
    eps_E=epso*eps_ferro+(Ps*(sech((E-Ec)/(2*dlt)))^2)/(2*dlt);
    cap_ferr= (eps_E*fer_area)/L;
    cap_den(i,2) = cap_ferr
    cap_den(i,1) = V(i)
end
plot(cap_den(:,1),cap_den(:,2),'-b');
xlabel('Anode Voltage (V)');
ylabel('Capacitance (F)');
```



## Appendix P: MATLAB Code for Small-Signal Capacitance Hysteresis

```

clc;
clear all;
close all;
%%%%%
format long;
load Expt2.dat;
expt_vol = Expt2(:,1);
expt_pol = Expt2(:,2);
load Expcapa1.dat;
expv=Expcapa1(:,1);
expc=Expcapa1(:,2);
%%%%%%%%%
area=5*10^-8;      % AREA in m^2 %
eps_ferro=10;      % Relative Permittivity of P(VDF-TrFE)
ee0=8.8541e-12;    % permittivity of free space (F/m)
T=210e-9;          % thickness in m
Cc=(area*ee0*eps_ferro)/T;
f=1*10^6           % frequency in Hertz
y=2e3              % viscosity coefficient
w=2*pi*f;
RS=(y*T)/area;
%EC=(5.145e5)*(1e2); %V/m original
EC=(4.145e5)*(1e2); %V/m
z=0.2              % E3=EC(1+z)
z4=0.2             % E3=EC(1+z4)

Vcon=(1+z)*EC*T
Vconneg=(1-z4)*EC*T
PRneg=-(7.41*10^-6)*(1*10^4); %C/m^2 negative remnant polarization
PC=-(7.994*10^-6)*(1*10^4); %C/m^2 polarization at negative coercive field
P3=(7.68*10^-6)*(1*10^4); %C/m^2 polarization at V3 at Vcon
P4=-(5.42*10^-6)*(1*10^4); %C/m^2 polarization at V4 at Vconneg
PUP=(8.460834961*10^-6)*(1*10^4); %C/m^2 max pol or spontaneous pol
pvec= [PC PRneg 0 P3 P4 ]/(1*10^4);
Vvec=[ -T*EC  0 T*EC  T*EC*(1+z) T*EC*(1-z4) ];
b=((3*(3^(1/2))*EC)/(2*PUP^3)) % beta
a=b*PUP^2 % alpha
% for calculation B1, B2, B3 and B4
r1=PRneg/PUP;
r2=PC/PUP;
r3=P3/PUP;
r4=P4/PUP;

```

## Appendix P (Continued)

```

aup1=(1+r1)/2;
aup2=(1+r2)/2;
aup3=(1+r3)/2;
aup4=(1+r4)/2;

x1=tan(pi*(aup1-0.5))
x2=tan(pi*(aup2-0.5))
x3=tan(pi*(aup3-0.5))
x4=tan(pi*(aup4-0.5))
% x= B1*(EFIELD -EC)+ B2*(EFIELD -EC)^2* u( E-EC) + B3*(EFIELD-EC)^2
u(EC-E) + B4*(EFIELD -EC)^3

%EField=0;
%x1= -EC* B1 + B2*0 B3*(-EC)^2) + B4*(0-EC)^3
%EField=-EC;
%x2= - 2*B1*EC + B2*0 B3*(-2*EC)^2) + B4*(-2*EC)^3 ;
% EFIELD= EC(1+z)
%x3= z* B1*EC + B2*(z*EC)^2 + B3*0 + B4*(z*EC)^3
% EFIELD= EC(1-z)
%x4= -z* B1*EC + B2*0 + B3*(-z*EC)^2 + B4*(-z*EC)^3
%%%%%%%%%%%%
%finding B1, B2, B3, B4 using inverse matrix method

A=[-EC 0 (-EC)^2 (-EC)^3;
-(2*EC) 0 (-2*EC)^2 (-2*EC)^3 ;
z*EC (z*EC)^2 0 (z*EC)^3;
-z4*EC 0 (-z4*EC)^2 (-z4*EC)^3];
I=inv(A)
X=[x1; x2; x3; x4]

B=I*X
B1=B(1)
B2=B(2)
B3=B(3)
B4=B(4)
%%%%%%%%
Vo=20;
Vmax=Vo;
Vmin=-Vo;
N=1000;
stair=0:N; % sequence starts at zero and ends on N
une=ones(size(stair));
V=Vmin*une+ (Vmax-Vmin)/N*stair; % allowed values for V

```

## Appendix P (Continued)

```

Efield=V/T; % allowed electric field values

up= 0.5*( (sign(Efield-EC*une))+une);
um=0.5*( (sign(EC*une-Efield))+une);

x= B1*(Efield-EC)+ B2*(Efield -EC).^(2*une).*up + B3*(Efield-EC).^(2*une).*um +
B4*(Efield -EC).^(3*une);
aup= (atan(x)+une*pi/2)/pi;
P=(2*aup-une)*PUP;
PP=P*1e-4; % in C/cm2

plot( V, PP, 'x')
hold on;
plot( V, PP, Vvec, pvec, 's');

for m=1:N+1
    plot (V(m), PP(m), 'b*')
    FP(m)=-PP(m); % flipping polarization value
    hold on;
end;
xlabel('Anode Voltage (V)');
ylabel('Polarization (C/cm^2)');

for m=1:N+1
    VV(m)=V(N+2-m);
end;
plot( VV, FP, 'x')
hold on;
plot(expt_vol, expt_pol, 'r^');
box on;
grid on;
for m=1:N+1
    %for capacitance
    xx(m)=1./(1+(x(m).^2));
    y(m)=B1+(2.*B2.*((Efield(m)-EC).*up(m)))+(2.*B3.*((Efield(m)-
EC).*um(m)))+(3.*B4.*((Efield(m)-EC).^2));
    daupdv(m)=(xx(m).*y(m))./(pi.*T);
    C(m)=Cc+(2.*area.*PUP.*daupdv(m));
    %% for small signal capacitor
    Q(m)=area.*((ee0.*eps_ferro.*Efield(m))+P(m)); %% charge
    term(m)=area./(T.*(a+(3.*b.*((Q(m)./area).^2))));
    term2(m)=(1+(RS.*w.*term(m)));

```

## Appendix P (Continued)

```
Csmall(m)=area./((T.*(a+(3.*b.*((Q(m)./area).^2))))+(area.*RS.*w));
end;
figure(2); %capacitance plot
plot(V,C,'bx');
hold on;
plot(VV,C,'bx');
plot(expv,expc,'r^');
box on;
xlabel('Anode Voltage (V)');
ylabel('Capacitance (F)');
grid on;

figure(3); %capacitance plot
plot(V,Csmall,'bx');
hold on;
plot(VV,Csmall,'bx');
hold on;
plot(expv,expc,'r^');
xlabel('Anode Voltage (V)');
ylabel('Capacitance (F)');
```